John von Neumann Institute for Computing

Phase Behavior and Chain Conformations in Polymer Blends: Monte Carlo Simulation vs Mean Field Theory

Marcus Müller

published in

Computational Soft Matter: From Synthetic Polymers to Proteins, Lecture Notes,
Norbert Attig, Kurt Binder, Helmut Grubmüller, Kurt Kremer (Eds.),
John von Neumann Institute for Computing, Jülich,
NIC Series, Vol. **23***, ISBN 3-00-012641-4, pp. 237-274, 2004.*

http://www.fz-juelich.de/nic-series/volume23

Phase Behavior and Chain Conformations in Polymer Blends: Monte Carlo Simulation vs Mean Field Theory

Marcus Müller

Institut für Physik, Johannes Gutenberg-Universität,
55099 Mainz, Germany
E-mail: marcus.mueller@uni-mainz.de

Using Monte Carlo simulations we investigate the phase behavior and interface properties in incompressible binary polymer blends. Special attention is focused on the relation between the Flory-Huggins parameter χ, that describes the incompatibility of the monomeric units in the mean field theory, and the particle-based model used in the simulations. The role of chain conformations on the thermodynamics and structure of the blend is investigated. We present a quantitative comparison between Monte Carlo simulations and mean field theory and the role of fluctuations in the bulk and at interfaces is explored.

1 Introduction

Melt blending of polymers is a promising route for tailoring materials to specific application properties: Polymeric materials in daily life are generally multicomponent systems. Chemically different polymers are "alloyed" as to design a material which combines the favorable characteristics of the individual components.[1] Clearly the miscibility behavior of the blend is crucial for understanding and tailoring properties relevant for practical applications. Miscibility on a microscopic length scale is desirable for a high tensile strength of the material. Unlike metallic alloys, however, chemically different polymers often do not mix on microscopic length scales. Rather a complicated morphology of droplets of one component dispersed into the other component forms on a mesoscopic length scale, and the blend can be conceived as an assembly of interfaces. While the detailed structure on this mesoscopic length scale depends strongly on the way the material is processed, the local properties of interfaces are certainly crucial for understanding the material properties. For instance, the interfacial width sets the length scale on which entanglement between polymers of the different components form. Experiments[2] suggest that the mechanical strength increases if the interfacial width exceeds the entanglement length. Alternatively, the interfacial tension is important for the breaking–up of droplets under shear:[3,4] The lower the interfacial tension is the finer are dispersed the two components.

In the following we consider a dense incompressible mixture of two components A and B. Upon increasing the incompatibility between the two species the mixture will phase separate into an A-rich and a B-rich liquid. Of course, in compressible mixtures more complex phase behavior can occur. In fact, six qualitatively different types of phase diagrams can be distinguished for compressible binary mixtures according to a scheme by Konynenburg and Scott.[5] In the following we restrict our attention to liquid-liquid immiscibility, which is characterized by a single order parameter, ϕ, being the composition of the mixture.

Much of the qualitative behavior of dense multicomponent polymer systems can be understood from a coarse-grained description: The large size of the chain molecules imparts a

rather universal behavior onto dense polymer mixtures, which can be characterized by only a small number of parameters: the end-to-end distance R_e of the molecules, and the incompatibility per chain, χN. The Flory-Huggins parameter χ describes the repulsion between unlike segments and N is the number of segments per molecule. R_e sets the characteristic length scale of spatial inhomogeneities, e.g., the width of interfaces between coexisting phases. Since this length scale is much larger than the size of the repeat units along the backbone of the polymer chain, one can use the Gaussian chain model, which captures the long-wavelength behavior of the polymer conformations in a melt. The parameters, R_e and χN, encode the chemical structure of the polymer on microscopic length scales. The properties on the mesoscopic length scale do depend on the microscopic structure only via the parameters R_e and χN.

Even in simple cases, the Flory-Huggins parameter χ results from small differences of dispersion forces between the different chemical segments and is typically only of the order $10^{-2} - 10^{-4}$ per segment. The extension of a polymer in a homogeneous melt results from a delicate screening of excluded volume interactions along the chain by surrounding molecules, and R_e depends on the density and temperature. Deriving those coarse-grained parameters, R_e and χN, from a microscopic model (e.g., atomistic force fields) is a formidable task. When these coarse-grained parameters are determined independently (e.g., by experiments) and used as an input, however, coarse-grained models are successful in making quantitative predictions.

Coarse-grained, particle-based models represent chains as a string of bonded segments on a lattice interacting via potentials of finite range. Field theoretical models represent chains as Gaussian walks in continuum space with end-to-end distance R_e and zero-ranged segmental repulsions of strength χ. By virtue of universality both are expected to yield identical descriptions for properties on mesoscopic length scales.

Computer simulations of coarse-grained, particle-based models numerically investigate the structure and thermodynamics without any approximation. Studies of the field theoretical model often invoke a mean field approximation: The self-consistent field (SCF) theory[6–10] neglects fluctuations of the composition in the multicomponent system. Due to the extended shape of the molecules, one molecule interacts with many neighbors, and the mean field approximation is quite accurate under many circumstances. Let us introduce the quantity $\sqrt{\mathcal{N}} = \Phi R_e^3$, where Φ denote the polymer number density. This quantity characterizes the number of molecules inside the volume of the reference chain. It measures the degree of interdigitation of the molecules. In a dense melt, $\mathcal{N}$ is proportional to the number of segments N per chain. For systems which differ in $\mathcal{N}$ but are characterized by the same coarse-grained parameters, χN and R_e, the SCF theory will make identical predictions. The quantity $\mathcal{N}$ plays an important role as it controls the strength of fluctuations.

Of course, one can describe the properties of the blend also by the characteristics on the scale of monomeric units: The number of segments N, the statistical segment length $b = R_e^2/N$, the Flory-Huggins parameter χ, and the monomer density $\rho = \Phi/N$. However, the results must not change upon representing the chains by a different number of effective segments N'. Such a reparameterization leaves the combinations χN, R_e and $\mathcal{N}$ invariant.

We can address two types of questions by quantitatively comparing computer simulations of coarse-grained, particle-based polymer models with SCF theory: (**i**) How to identify the coarse-grained parameter, χN, for a specific, particle-based model? For which properties and parameters is the coarse-grained description of the polymer conformations

by the Gaussian chain model is valid? For which aspects are microscopic properties of the underlying model important? (**ii**) What is the validity of the mean field approximation (or additional approximations invoked in less accurate analytical treatments of the field theoretical model)?

In the following we shall describe computer simulations in the framework of a coarse–grained lattice model targeted at investigating the phase behavior and the local structure of the interfaces in polymer blends and systems containing diblock copolymers. The results are compared to SCF calculations. In the next section we provide some background on the qualitative behavior of these systems. Then, we describe our computational model and the Monte Carlo (MC) technique. Subsequently, we detail our results on symmetric binary blends, binary blends of polymers with different stiffness, a ternary blend of two homopolymers and a symmetric diblock copolymer.

2 Background

2.1 Bulk Phase Behavior of a Binary Blend: Flory-Huggins Theory

We consider a dense mixture of polymers that comprises to species - A and B. Each molecule comprises N segments, and unlike segments repel each other with strength χ. The free energy of mixing per molecule takes the form:

$$\frac{F_{\mathrm{FH}}(\phi)}{T\Phi V} = \phi \ln \phi + (1-\phi)\ln(1-\phi) + \chi N \phi (1-\phi), \tag{1}$$

where Φ denotes the number density of polymers and ϕ the composition of the incompressible mixture. T is the temperature and we set Boltzmann's constant $k_B = 1$. The first two terms describe the entropy of mixing; it stems entirely from the translational entropy. The last term describes the energy of mixing per molecule. Note that this Flory-Huggins free energy[11] does not include any contribution from the conformational entropy of the extended macromolecules. Implicitly, one assumes that the conformations of a single chain in a homogeneous system are independent from the environment (i.e., local composition and temperature).

When χ is used as an adjustable parameter or extracted from experiments, this mean field theory[11] of Flory and Huggins is quite successful in describing many experimental observations. Most notably the theory rationalizes the fact that long macromolecules tend to demix at very high temperatures. The critical point of the blend is located at:

$$\frac{N}{T_c} \sim \chi_c N = 2 \qquad \text{and} \qquad \phi_c = \frac{1}{2}\,, \tag{2}$$

The Flory-Huggins theory provides simple analytical expressions for the free energy of mixing. This simple form of the bulk free energy lays at the basis of SCF calculations[6–10] for spatially inhomogeneous polymer systems in the framework of the Gaussian chain model. Nevertheless, the Flory-Huggins theory cannot rationalize the following observations:

(**i**) The temperature dependence of the measured values on the χ parameter often takes the form $\chi = A + B/T$. Following a common convention, B is denoted as the enthalpic

contribution, whereas A is referred to as an additional entropic contribution. In the framework of the Flory-Huggins theory,[11] the only contribution to the entropy of mixing stems from the translation of the molecules as a whole. Hence, the entropy of mixing per polymer is of the order unity. Additional entropic contributions e.g., due to the dependence of the packing arrangement of the segments on the local environment, may become important. In experiments, however, the temperature dependence of χ is only accessible over a rather small temperature range and there is a strong interplay between entropic and enthalpic contributions, which makes the standard decomposition of χ into an entropic and an enthalpic part difficult: e.g., the temperature dependence of the chain conformations or equation of state effects might yield a nonlinear relation between χ and the inverse temperature. Moreover, the χ parameter often depends on composition and chain length as well.

(**ii**) According to the original mean field theory, the demixing temperature is independent of the molecular architecture. Hence, blends of two homopolymers and two ring or star polymers with the same number of monomeric units are predicted to have the same miscibility behavior. Similarly, the theory does not capture the dependence of the miscibility behavior of the chain stiffness or the degree of branching.[12,13]

(**iii**) Being a mean field theory, the Flory-Huggins theory neglects fluctuations of the local composition and invokes a random mixing approximation. Thus, the behavior in the vicinity of the critical point is described by mean field exponents and the binodals have a parabolic shape. In the ultimate vicinity of the critical point, the correlation length grows very large and the polymeric properties become irrelevant. In this critical region the behavior is characterized by the 3D Ising universality class[14] which applies to all binary mixtures with short-ranged interactions. The latter behavior manifests itself in a much flatter binodal at the critical point and a stronger divergence of composition fluctuations. This has been observed in neutron scattering experiments extremely close to the critical point.[15,16]

(**iv**) The same intermolecular forces which determine the miscibility behavior alter the conformation of the extended flexible macromolecules. MC simulations[14,17–22] for rather short chain lengths reveal a contraction of the polymer coils in the minority phase. Experiments in highly incompatible poly(methyl methacrylate) (PMMA) and poly(vinyl acetate) (PVAc) blends of rather low molecular weight indicate a relative contraction of isolated PMMA chain extensions by 13-15%.[23] These observations indicate a possible coupling between the single chain conformations and the thermodynamic state (i.e., temperature and composition of the mixture).

2.2 Interfaces Between Coexisting Phases: SCF Theory

In spatially inhomogeneous systems, the structure of the polymer molecules becomes more apparent. The SCF theory considers a mixture of Gaussian chains with end-to-end distance R_e. The statistical mechanics of the interacting multi-chain system is analytically intractable and therefore one invokes a mean field approximation: The interaction of an A-chain with its neighbors is approximated by an effective external field $W_A[\phi]$, that depends, in turn, on the local composition $\phi(\mathbf{r})$. Then, the local density of A-chains is calculated as the Boltzmann average of the single chain density in the external field, and likewise for B-polymers. This relation and $W_A[\phi]$ constitute a closed self-consistent set of equations, which allows to describe inhomogeneous systems.[6–10]

The single chain problem in the spatially varying external field can be solved only numerically. Using the Gaussian chain model, one has to deal with a modified diffusion equation. Alternatively, one can solve the single chain problem by brute force, partially enumerating the polymer configurations. To this end, one extracts a large number of A-chain conformations (typically $10^7 - 10^8$) from the simulations and calculates the Boltzmann average of the conformations in the external field W_A, and does likewise for B-chains.[24,25] This method has the advantage of describing the chain conformations on all length scales (including the rod-like behavior and/or self-avoiding walk like behavior on small length scales), but it is considerably more involved computationally.

In some limiting cases simple analytic expressions can be obtained:

(**i**) In the vicinity of the critical point, the variation of the composition can be treated as a small parameter. Expanding the spatial variation of the composition in a Fourier-basis, $\phi(\mathbf{q}) = \phi_A(\mathbf{q}) = -\phi_B(\mathbf{q})$ for $q \neq 0$, and only considering terms to quadratic order, one derives the random phase (RPA) approximation for the free energy per molecule:[26]

$$\frac{F_{\mathrm{RPA}}[\phi(\mathbf{q})]}{T\Phi V} = \frac{1}{2}\sum_{\mathbf{q}} \phi(\mathbf{q}) \left\{ \frac{1}{\phi g(\mathbf{q})} + \frac{1}{(1-\phi) g(\mathbf{q})} \right\} \phi(-\mathbf{q}) - \frac{1}{2}\sum_{\mathbf{q}} \phi(\mathbf{q}) 2\chi N \phi(-\mathbf{q}) \ , \tag{3}$$

where the Debye function g characterizes the single chain structure factor of a Gaussian chain

$$g(\mathbf{q}) = \frac{12}{q^2 R_e^2} \left(\exp\left[-q^2 R_e^2/6\right] - 1 + q^2 R_e^2/6 \right) \ . \tag{4}$$

The first two terms in Eq.(3) represent the conformational entropies of the two polymer species, the last term is the energy of mixing.

Calculating fluctuations of the composition around the homogeneous phase above the unmixing transition temperature, we obtain for the correlation length ξ

$$\frac{\xi}{R_e} = \frac{1}{\sqrt{18[1 - 2\chi N \phi(1-\phi)]}}. \tag{5}$$

For larger incompatibilities $\chi N > \chi_c N = 2$, the blend phase separates into an A-rich and a B-rich bulk. The two phases are separated by an interface, which is described by a tanh-profile

$$\phi(z) = \frac{1}{2}\left(1 + \tanh[z/w_{\mathrm{WSL}}]\right) \qquad \text{with} \qquad w_{\mathrm{WSL}} = 2\xi \tag{6}$$

In the weak segregation limit (WSL) a polymer mixture behaves similar to a mixture of small molecules, because the characteristic size of composition variations is on the order of the molecular extension R_e, and therefore the Gaussian conformational statistics is not important, only the overall size of the molecule matters.

(**ii**) Far below the critical temperature, $\chi N \gg 2$, the SCF calculations take a particularly simple form (ground state dominance). In this case, the entropy loss the chain suffers at a spatial inhomogeneity can be described by the Lifshitz formula:[27]

$$\frac{S[\phi]}{T\Phi V} = -\frac{R_e^2}{24V} \int \mathrm{d}^3\mathbf{r} \ \left\{ \frac{(\nabla\phi)^2}{\phi} + \frac{(\nabla(1-\phi))^2}{1-\phi} \right\} \tag{7}$$

In this case the interface profile, $\phi(z)$, is also described by the tanh-profile like in Eq.(6), but with a width

$$\frac{w_{\rm SSL}}{R_e} = \frac{1}{\sqrt{6\chi N}} \tag{8}$$

This result can be heuristically understood as follows: The properties of the interface are dominated by excursions of A-polymers into the B-rich phase, and vice versa. The energy cost of each loop is comparable to the thermal energy scale T. Each monomer of a loop contributes to the energy an amount of the order χT, and, consequentially, the number of monomers per loop scales as $1/\chi$. The spatial extension of the loops determines the interfacial width. In the Gaussian chain model the conformational distribution is Gaussian on all length scales, and therefore the spatial extension of loops is on the order of $R_e/\sqrt{\chi N}$. Each monomer in the interfacial region contributes to the interface tension an amount χ, and the interface tension scales as $\chi\Phi N R_e/\sqrt{\chi N}$. The final result (including prefactor of order unity) is:

$$\frac{\sigma_{\rm SSL} R_e^2}{T} = \sqrt{\mathcal{N}}\sqrt{\frac{\chi N}{6}} \tag{9}$$

In the strong segregation limit (SSL) loops determine the interface properties, which depend sensitively on the conformational statistics of the molecule. The SCF theory describes both limits, (**i**) WSL and (**ii**) SSL, and the crossover between them.

3 Models and Techniques

Simulations of the miscibility behavior in polymer blends are considerably more exacting in computational terms than those of small molecules or magnetic systems. The problems stem from the difficulty of dealing with the widely spread time and length scales caused by the extended structure of the macromolecules. Therefore coarse–grained models are promising candidates for investigating the universal, qualitative characteristics of miscibility. Introducing specific structural modifications or asymmetries, we can highlight their influence on the miscibility behavior. A detailed comparison between different computational models is warranted to investigate the degree of universality of the observed effects and to explore the effects of structure on various length scales. Simulational models of various degree of coarse–graining have been employed, ranging from the representation of polymers as self avoiding walks on a simple cubic lattice – as in the original treatment of Flory and Huggins[11] – to simulations of the effect of branching in hydrocarbon melts in the framework of a united atom model.[28] The choice of the simulation model is a compromise between computational efficiency and a more faithful representation of the details of molecular architecture.

We shall present MC simulations in the framework of the bond fluctuation model,[29] which incorporates the relevant universal characteristics of polymer blends: Connectivity of the monomers along a chain, excluded volume of the segments, and a thermal interaction between monomers. In the framework of this coarse–grained lattice model, a monomer occupies the 8 corners of a unit cell from further occupancy. Monomers along a polymer are connected by one of 108 bond vectors of length $2, \sqrt{5}, \sqrt{6}, 3$, and $\sqrt{10}$. The bond vectors are chosen such that the excluded volume interactions prevents a crossing of bond

vectors during the motion. Therefore the algorithm captures the effect of entanglements. The large number of bond vectors allows for 87 different bond angles – an indication for the rather good approximation of continuous space properties by this complex lattice model. This property also allows for a rather realistic implementation of the bending rigidity.

Here and in the following all length scales are measured in units of the lattice spacing. When atomistically detailed simulations are mapped onto the bond fluctuation model a lattice unit corresponds to roughly 2 Angstrom and a monomer in the bond fluctuation model represents a small number – say 3 to 5 – of chemical repeat units.[30] If not noted explicitly, we work at a monomer number density of $\rho \equiv \Phi N = 1/16$, i.e., due to the extended structure of the monomers half of the lattice sites are occupied. These parameters correspond to a concentrated solution or a melt. On the one hand the presence of vacancies allows a reasonably fast equilibration of the chain conformations on the lattice. On the other hand the size disparity between vacancies and extended monomers gives rise to packing effects. Indeed, the monomer–monomer density pair correlation function $g(\mathbf{r})$ exhibits oscillations at small distances indicating a fluid–like packing due to the local compressibility. Moreover, the relation between osmotic pressure and density is well describable via the Carnahan-Starling equation[31] - an approximation for the equation of state of hard spheres. This exemplifies that this lattice model shares many features with off–lattice models.

The conformations of the polymers on the lattice evolve via local random monomer hopping[29] – a randomly chosen monomer attempts to move one lattice constant in a random direction – or slithering snake-like moves[32,33] – a segment of the chain is removed at one end of the chain and added at the opposite one. While the former allows for a dynamical interpretation of the MC simulations in terms of a purely diffusional dynamics,[29] the latter relaxes the chain conformations a factor N faster.

The blends comprise two components – denoted A and B. Monomeric units of the same type attract each other whereas different monomers repel each other via a square well potential

$$\epsilon = -\epsilon_{AA} = -\epsilon_{BB} = \epsilon_{AB} \ . \tag{10}$$

The potential is extended over the first peak of the pair correlation function, i.e., it incorporates the first 54 neighbors up to a distance $\sqrt{6}$. The form of the potential is chosen by computational convenience; we expect our results to be qualitatively independent from the specific potentials used. However, if we were to model the interactions as (strongly) attractive with (slightly) different strengths between unlike species – a more faithful modeling of interactions in view of the experiment situation – the presence of vacancies would allow for a liquid-vapor phase separation between a concentrated polymer melt and a dilute phase in our ternary system. This liquid-vapor phase separation is common to both lattice based models and models in continuous space. The temperature scale of this liquid-vapor coexistence is set by the Θ temperature, which is chain length independent. This contrasts with the temperature scale of the liquid-liquid phase separation into A-rich and B-rich phases with similar content of vacancies. The latter temperature scale increases linearly with the chain length. Therefore, the two phenomena are well separated in blends of high molecular weight. In this paper we focus on the liquid-liquid phase separation at high temperatures.

In the following, we identify the Flory-Huggins parameter χ via the energy of mixing:

$$\chi N = \Phi N^2 \int \mathrm{d}^3\mathbf{r} \left[g_{AB}^{\mathrm{inter}}(\mathbf{r}) v_{AB}(\mathbf{r}) - \frac{g_{AA}^{\mathrm{inter}}(\mathbf{r}) v_{AA}(\mathbf{r}) + g_{BB}^{\mathrm{inter}}(\mathbf{r}) v_{BB}(\mathbf{r})}{2} \right] \quad (11)$$

$$= \frac{2 N z_c \epsilon}{T} \qquad \text{with} \qquad z_c = \Phi N \int_{r \leq \sqrt{6}} \mathrm{d}^3\mathbf{r}\; g^{\mathrm{inter}}(\mathbf{r}) \quad (12)$$

where v_{IJ} $(I, J = A, B)$ denote the interaction potentials between the different segments. $g_{IJ}^{\mathrm{inter}}(\mathbf{r})$ denotes the intermolecular paircorrelation function, which describes the probability to find a monomer of type J that belongs to a different chain a distance $\mathbf{r}$ away from a monomer of type I. In analogy to the original treatment of Flory and Huggins we refer to z_c as the effective coordination number. This equation expresses the χ parameter in terms of observables that are directly accessible in the MC simulations. Moreover, we shall often approximate the intermolecular pair correlation functions by their athermal values. It is not that the total number of interactions determine the miscibility behavior, but rather the intramolecular interactions do not contribute. Even in this simple form it is evident that the chain architecture has pronounced effects on the intermolecular paircorrelation function and the miscibility behavior: The more open the chains are, the larger is the number of intermolecular contacts, and the smaller is the miscibility.

Being a lattice model, the bond fluctuation model is highly computationally efficient. It allows for the investigation of rather large chain lengths and large system sizes. The latter is necessary to accurately locate the critical temperature via finite size scaling analysis. As we shall illustrate, the large chain length is crucial for reaching the high molecular weight scaling limit and extrapolating some quantities to experimentally relevant chain lengths. For the present investigation chains with up to 512 (2048 for athermal systems) monomeric units have been employed.

Various simulation techniques have been used for exploring the miscibility properties of polymer blends. The most direct one is the simulation of both the coexisting phases in the simulation cell. This method has been employed by Madden[34] and Cifra[35] for well segregated blends, and it also yields information about interfacial properties. However, it requires rather large simulation cells in order to extract "bulk" properties. Especially, the scheme is not very well suited to cope with the growing of the correlation length and vanishing of the difference between the phases as the critical point is approached. Computationally more efficient seems the direct estimation of the chemical potential of each individual species as a function of temperature and composition. At coexistence the chemical potentials of the species in both phases are equal and the coexistence curve can be mapped out. This technique has been applied successfully by Kumar[36] using the incremental chemical potential method.[37] Kumar explored the influence of pressure and compressibility on the miscibility behavior. If one point on the coexistence curve is known, a Gibbs Duhem integration technique can be employed to obtain the coexistence under constant pressure conditions.[38,39] Both methodologies are particularly useful for blends in which the constituents are characterized by very different chain architecture.

Sariban and Binder[14] employed simulations in the semi-grandcanonical ensemble for investigating the phase behavior at constant volume. In this ensemble, the total monomer density is fixed, the composition of the blend fluctuates, and the chemical potential difference $\Delta\mu$ between the species is controlled. The MC scheme comprises two types of moves. Canonical updates relax the conformation of the macromolecules on the lat-

tice, whereas semi-grandcanonical ones transfer A polymers into B polymers and vice-versa. Sariban and Binder investigated strictly symmetric chains, for which the semi-grandcanonical moves consists in a mere exchange of labels. The algorithm can be extended to some degree of structural asymmetry (e.g., different chain lengths between the species[32]). Overall speaking, it is reasonably efficient for a modest degree of structural asymmetry between the different constituents, but the extension to pronounced structural asymmetries is a challenging task. Improvement might be achieved via gradually "mutating" one species into another.[40] The major advantages of the methodology stem from the fluctuation of the composition of the mixture:

(**i**) The relaxation times are much smaller than in the canonical ensemble, where the composition is conserved and composition fluctuations decay via the slow diffusion of polymers in a melt. The semi-grandcanonical ensemble allows the straightforward application of finite size scaling techniques known from simple mixtures. Therefore we can measure the critical temperature in symmetric and asymmetric mixtures accurately from the MC simulations of modest system size. (**ii**) Moreover, the SG–EOS which relates the composition of the mixture to the difference of the chemical potentials of the species is directly accessible with high accuracy. The latter is particularly important to establish a direct contact to analytical approaches outside of the ultimate critical region where 3D Ising critical behavior dominates – i.e., in the region where the mean field theories are applicable. (**iii**) Additionally, it is possible to determine excess interfacial properties (e.g., interfacial tension,[41] excess energy,[42] enrichment of a third component[42]).

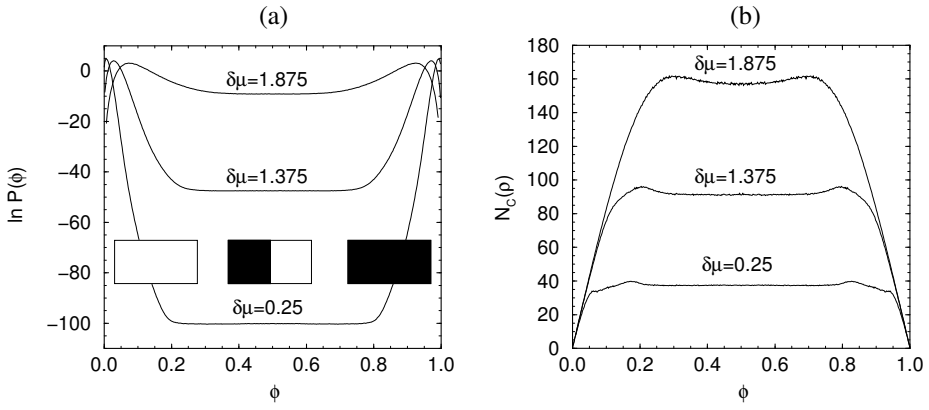

Figure 1. Ternary blend containing two homopolymers A and B and a symmetric AB diblock copolymer. (**a**) Probability distribution at $\epsilon = 0.054$ and system size $48 \times 48 \times 96$. Upon increasing the chemical potential $\delta\mu$ of the copolymers the "valley" becomes shallower, indicating that the copolymers decrease the interfacial tension. One clearly observes a plateau around $\rho = 1/2$. This assures, that our system size is large enough to neglect interfacial interactions in the measurement of the interfacial tension. (**b**) Average number of copolymers as a function of the composition. The copolymer number is enhanced in the configuration containing two interfaces. From Müller and Schick.[42]

An important quantity in the semi-grandcanonical simulations is the probability distribution of the composition $P(\phi)$. At phase coexistence, it exhibits two peaks that correspond to the two coexisting phases. At coexistence, the exchange chemical potential

$\Delta\mu = \mu_A - \mu_B$, conjugated to the composition, has to be chosen such that both peaks have equal weight. (For a symmetric blend, $\Delta\mu_{\rm coex} = 0$, of course).

At the critical point, the probability distribution adopts a universal shape when scaled to unit norm and variance. The shape characterizes the universality class to the transition. In case of unmixing this is the 3D Ising universality class. Adjusting the temperature (i.e., χN) as to match the probability distribution obtained from simulations and the predetermined universal curve, we accurately determine the critical temperature from the simulation.[43]

At lower temperatures, the system has to tunnel between the two coexisting states, which are separated by a large free energy barrier (cf. Fig. 1(**a**)). Therefore the probability of finding the system at $\phi_{\rm middle} = (\phi^{(1)}_{\rm coex} + \phi^{(2)}_{\rm coex})/2$ is very low. In the middle of the miscibility gap, the typical configuration consists of a slab of A-rich phase, which is separated by two interfaces of size L^2 from the B-rich phase. The probability of these configurations is suppressed by an amount $P_{\rm middle}/P_{\rm coex} = \exp(-2L^2\sigma/T)$. Thus, we not only obtain information about the coexisting phases (composition, susceptibility, and coexistence chemical potential), but also about interface properties. One can also monitor other quantities (e.g., the excess of a third species, see Fig. 1(**b**)) as a function of the composition and obtain the difference (excess) between the bulk and the system containing two interfaces.

In order to overcome the free energy barrier, one applies pre-weighting techniques: One adds to the original Hamiltonian $\mathcal{H}$ of the system a function $w(\phi)$ that depends on the composition, but not on the microscopic conformations of the polymers. The probability distribution of the pre-weighted system is given by:

$$P_{\rm pw}(\phi) \sim P_{\rm orig}(\phi)\ \exp(-w(\phi)/T) \tag{13}$$

Choosing $w(\phi) \approx T \ln P_{\rm orig}(\phi)$ the system samples all compositions with roughly equal probability. The crux is that the probability distribution $P_{\rm orig}$ is not known a priory; it rather is the result of the calculation. Several strategies have been devised to generate estimates to be used in simulation. (**i**) Histogram-reweighting techniques[44] alleviate this problem by performing a sequence of weighted simulations and extrapolations starting at a point where barriers are small and the system explores a wide range of composition. More sophisticated methods combine results of multiple histograms[45]. (**ii**) Multicanonical recursion[46] conducts a series of short trial runs. After each run, the pre-weighting factors w are adjusted until the simulation can access all pertinent values of composition. The weight factors can also be self-adjusted during the simulation[47–50]. However, detailed balance is violated in this process and separation of statistical and systematic errors becomes difficult. (**iii**) Weight factors can also be obtained from the transition probabilities between macrostates[51,52]. Alternatively, one can use successive umbrella sampling, thereby dividing the pertinent range of composition into smaller subintervals and exploring each successively.[53]

4 Results

4.1 Phase Behavior: Fluid Structure and Composition Fluctuations

4.1.1 Symmetric blends

The scaling of the critical temperature with chain length was studied by Deutsch and Binder[18] in the framework of the bond fluctuation model. In accord with the predictions of the Flory-Huggins theory,[11] the simulations exhibited a linear scaling of the critical temperature with chain length, which was also observed in carefully designed experiments.[54] This finding stimulated advances in the development of integral equation theories.[55] The crossover between the mean field behavior away from the critical point and the ultimate 3D Ising behavior at the critical point was unraveled via a sophisticated analysis of the MC data which coped simultaneously with finite size effects and the crossover from mean field to 3D Ising critical behavior.

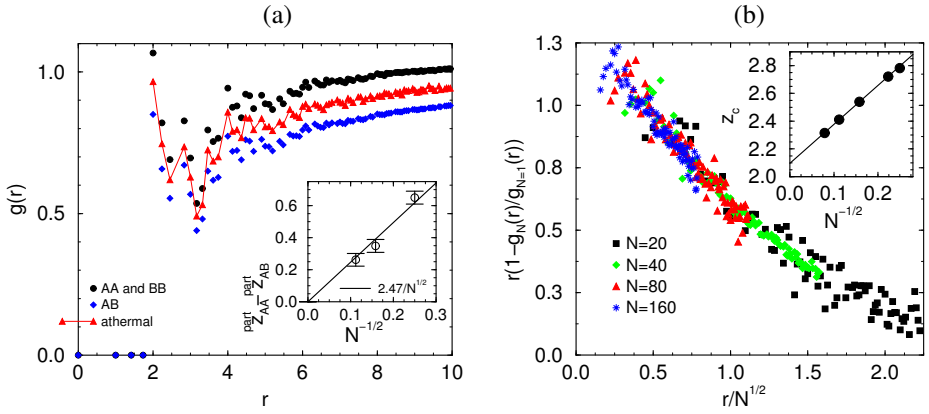

Figure 2.

(**a**) Intermolecular paircorrelation function for chain length $N = 80$ for the athermal system (triangles) and at criticality (circles and diamonds). The inset presents the scaling of the non-random mixing with increasing chain length. $z_{AA}^{\mathrm{part}} = \langle\phi\rangle \int \mathrm{d}^3\mathbf{r} g_{AA}^{\mathrm{inter}}(\mathbf{r})$. From Müller.[56] (**b**) Correlation hole of linear chains: Scaling behavior of the athermal intermolecular pair correlation function with chain length. The inset shows the chain length dependence of the effective coordination number. The line corresponds to $z_c = 2.1 + 2.8/\sqrt{N}$. From Müller and Binder.[32]

In order to relate the measured critical temperatures to the structure of the polymeric fluid,[32] we present in Fig.2(**a**) the intermolecular pair correlation function of strictly symmetric polymer blends in the athermal limit and at the critical point. In the athermal case, the distinction between the two species becomes irrelevant. The intermolecular pair correlation function mirrors two effects:[32] (**i**) Due to the extended monomer structure the pair correlation function vanishes for distances $r < 2$. The presence of vacancies introduces local packing effects, which give rise to a highly structured function at short distances. One

can identify several neighbor shells, which are characteristic of the monomeric fluid. These packing effects are, of course, absent in simple lattice models where a monomeric unit occupies a single lattice site and are less pronounced in the bond fluctuation model than in continuum models. The length scale of these packing effects is set by the monomeric extension or the statistical segment length; the detailed shape depends strongly on the model and the degree of structure on local length scales. (**ii**) Furthermore, the extended structure of the macromolecules manifests itself in a reduction of contacts with *other* chains on intermediate length scales.[26] The length of this polymeric correlation hole is set by the size of the molecules, R_e, and its shape is characteristic for the large scale conformations of the molecule.

To a first approximation, we assume that the fluid structure is determined by the packing of the hard cubes on the lattice; neither the connectivity of the monomers along a polymer nor the thermal interactions influence the total pair correlation function. Under this assumption, we can separate the fluid-like packing effects on the monomer scale and the polymeric correlation hole effect and approximate the intermolecular pair correlation function by:[32]

$$g^{\text{inter}}(r) = g_1(r) \left(1 - \frac{1}{\sqrt{\mathcal{N}}} f(r/R_e)\right) \tag{14}$$

where g_1 denotes the pair correlation function of the monomer fluid and the function f parameterizes the structure of the molecule on the scale R_e. The prefactor is determined by requirement that the correlation hole contains one polymer:

$$\Phi \int \mathrm{d}^3\mathbf{r} \, \left(\frac{g^{\text{inter}}(r)}{g_1(r)} - 1\right) = 1 \tag{15}$$

Indeed, this factorization works excellently for flexible molecules in the bond fluctuation model. The ratio $g^{\text{inter}}(r)/g_1(r)$ is largely independent of packing effects and permits a distinction between monomeric packing effects and polymeric correlation hole effects in the simulations – though the length scales are not clearly separated for short chains. Not surprisingly, the correlation hole becomes deeper and wider as we increase the molecular weight. The scaling behavior of the correlation hole is shown in Fig.2(**b**) for linear athermal chains. It imparts a chain length dependence on the Flory-Huggins parameter or the effective coordination number, respectively. The effective coordination number is related to the short distance behavior of the intermolecular paircorrelation function $z_c \sim \Phi N \sigma_e^3 g^{\text{inter}}(\sigma_e)$, where σ_e describes the range of the thermal interactions. More quantitatively, we calculate:

$$z_c = \Phi N \int_{r \le \sqrt{6}} \mathrm{d}^3\mathbf{r} \; g^{\text{inter}}(r) = z_c^{\infty} \left(1 + \frac{\text{const}}{\sqrt{\mathcal{N}}}\right) \tag{16}$$

The scaling of the effective coordination numbers for flexible linear chains is presented in the inset of the panel (**b**). The effective coordination number approaches its limiting scaling behavior with a $1/\sqrt{\mathcal{N}}$ correction.

In Fig.2(**a**) we also present the intermolecular pair correlation functions g_{AA} and g_{AB} for chain length $N = 80$ close to criticality. In accord with intuition, AA contacts are more likely than AB ones and, hence, $g_{AA}^{\text{inter}} > g_{BB}^{\text{inter}}$. However, note that the sum of AA and

AB correlations can be well approximated by the intermolecular paircorrelation function $g^{\rm inter}_{\rm atherm}(\mathbf{r})$ in the athermal limit:

$$\frac{g^{\rm inter}_{AA}(\mathbf{r}) + g^{\rm inter}_{AB}(\mathbf{r})}{2} \approx g^{\rm inter}_{\rm atherm}(\mathbf{r}) \tag{17}$$

This relation shows that the weak difference in interactions between the monomers $\chi \sim 1/N$ does not alter the structure of the monomer fluid. The energy of the system is mainly determined by composition fluctuations. The approximative decoupling between density fluctuations/packing effects and composition fluctuations in our model makes it possible to use the athermal value of the intermolecular pair correlation functions in Eq.(11). This identification corresponds to the high temperature approximation in the framework of the P-RISM theory.[55] In this sense, the miscibility behavior in this model can be described to a good approximation by a purely enthalpic χ parameter.

The inset of Fig.2(**a**) presents the integral of the correlation functions over the range of the square well potential, i.e., $z^{\rm part}_{AA} = \langle\phi\rangle \int_{r\leq\sqrt{6}} {\rm d}^3\mathbf{r}\; g^{\rm inter}_{AA}(\mathbf{r})$ and similarly for $z^{\rm part}_{AB}$. The MC simulations show that the difference between the AA and AB contacts decreases like $1/\sqrt{N}$, when χN is held constant. This exemplifies that the mean field approximation (or random mixing assumption) is justified in the limit $\mathcal{N} \to \infty$.

The vanishing of composition fluctuations can be rationalized by estimating the scaling of non–random mixing effects with growing chain length. The strength of composition fluctuations in a volume V is of the order $1/\Phi V$. Expressing the composition fluctuations via the correlation functions, we obtain for a symmetric blend:

$$\begin{aligned} 1 \sim \Phi V(\langle\phi^2\rangle - \langle\phi\rangle^2) &\sim \Phi \int {\rm d}^3\mathbf{r}\;\left[\frac{g^{\rm inter}_{AA}(\mathbf{r}) + g^{\rm inter}_{BB}(\mathbf{r})}{2} - g^{\rm inter}_{AB}(\mathbf{r})\right] \\ &\sim \sqrt{\mathcal{N}} \int {\rm d}^3\mathbf{x}\;\left[\frac{g^{\rm inter}_{AA}(\mathbf{x}) + g^{\rm inter}_{BB}(\mathbf{x})}{2} - g^{\rm inter}_{AB}(\mathbf{x})\right] \qquad \text{with} \qquad \mathbf{x} = \mathbf{r}/R_e \end{aligned} \tag{18}$$

Therefore, we expect the difference in the AA and AB correlations to vanish like

$$g^{\rm inter}_{AA}(\mathbf{r}) - g^{\rm inter}_{AB}(\mathbf{r}) \sim 1/\sqrt{\mathcal{N}} \tag{19}$$

upon increasing the chain length. These mean field arguments are in agreement with P-RISM calculations by Yethiraj and Schweizer.[55]

The non-random mixing gives rise to a correction of the mean field critical temperature of the order $1/\sqrt{\mathcal{N}}$. This behavior is in agreement with the Ginzburg criterium[57]: The neglect of fluctuations is justified when the concentration fluctuations in one "correlation volume" of size ξ^3 are small compared to the composition difference between the two coexisting phases. Using the Flory-Huggins free energy, we obtain for the binodals in the vicinity of the critical point :$\phi = 1/2(1 \pm \sqrt{3(\chi-\chi_c)/\chi_c})$. The strength of composition fluctuations is determined by the second derivative of the free energy of mixing:

$$V\Phi(\langle\phi^2\rangle - \langle\phi\rangle^2) = \frac{1}{\frac{1}{\phi} + \frac{1}{1-\phi} - 2\chi N} \tag{20}$$

and the correlation length scales like $\xi \sim R_e/\sqrt{\chi N - 2}$ Using the above expressions, one obtains:

$$\chi N - 2 \gg {\rm Gi} \sim \frac{1}{\mathcal{N}} \tag{21}$$

for the mean field theory to be accurate. The Ginzburg criterion[57] states that composition fluctuations are important at the critical point, where simulations[14] and experiments[54,16] find 3D Ising critical behavior. However, unlike the situation in mixtures of small molecules, the temperature interval in which composition fluctuations are dominant is restricted to the ultimate vicinity of the critical point. General arguments[58] rationalize that fluctuations lead to an overestimation of the "true" critical temperature T_c in the mean field theory $T_c^{\rm MF}$ by an amount $(T_c^{\rm MF} - T_c)/T_c \sim 1/\sqrt{\mathcal{N}}$, in accord with the non-random mixing behavior discussed above.

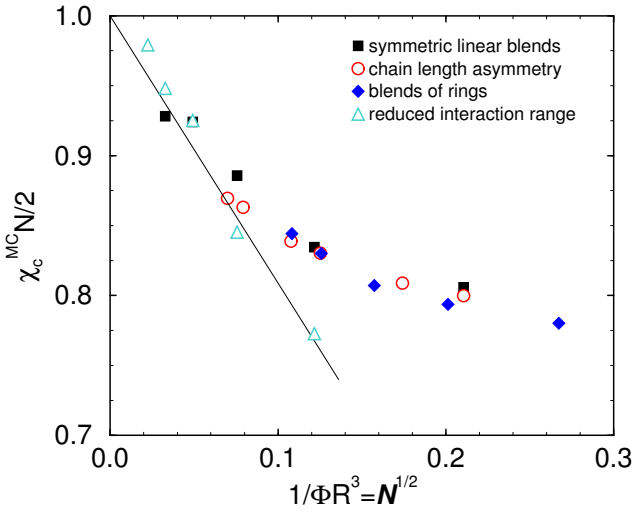

Figure 3. Ratio of the critical temperature (as determined in MC simulations) and the Flory-Huggins estimate for binary blends. Using the scaling variable $\sqrt{\mathcal{N}}$ the MC results for blends of linear chains and ring polymers collapse onto a common curve. From Müller.[56]

The linear scaling of the critical temperature at constant density has been observed for symmetric[18] and asymmetric[32] chains, and the behavior is also reproduced in off-lattice models.[59,60] The overestimation of the critical temperature is investigated in more detail in Fig.3. Here, we plot the ratio between the MC results and our simple mean field estimate of the critical temperature. Upon increasing the chain length the difference between the MC result and the mean field estimate decreases. The figure includes the ratios between the critical temperature and the mean field estimate for mixtures of different chain lengths and blends of ring polymers. Using the scaling variable $1/\sqrt{\mathcal{N}}$ we achieve a collapse of all data onto a common curve within the accuracy of the MC data which is of the order $1-5\%$. The figure also displays results for two choices of interactions ranges (for symmetric linear chains).[18] Circles represent the results of a model, where the square well potential is extended over the first 54 lattice sites (as in the remainder of this paper), while triangles denote the results of a model, where the interaction comprises only the 6 nearest lattice sites. For large chain lengths the MC results are consistent with a linear dependence on the scaling variable. The collapse of the ratio $T_c/T_c^{\rm MF}$ with $\sqrt{\mathcal{N}}$ for all blends marks the regime of chain lengths where the universal polymeric behavior dominates. This universal behavior is indicated as a straight line.

The bending towards a constant value of $T_c/T_c^{\rm MF}$ for small chains is due to the following effect: The deviations from the mean field behavior depend on the correlation length

ξ. The length scale is set by the amplitude of the square gradient term in the expansion of the free energy per chain with respect to long-ranged composition fluctuations. In a symmetric polymer mixture the prefactor is of the form $R_e^2/36\phi(1-\phi)$. Hence, the free energy cost of an inhomogeneous composition is due to the configurational entropy. However, for finite–ranged interactions there is an enthalpic contribution to the square gradient term with a prefactor of the order $\chi N\sigma_e^2$, where σ_e denotes the range of the monomeric interaction potentials. For long chain lengths the entropic contribution dominates, while the enthalpic term becomes important when the range of the thermal interactions becomes comparable to the radius of gyration of the chains. Consequently, the range of the interactions does not enter the Ginzburg criterion[57] to leading order. For very small polymers or rather long-ranged monomeric interactions, the interaction range σ_e might increase the correlation length and the shift between mean field and true critical temperature is smaller than estimated by $1/\sqrt{\mathcal{N}}$. When the range of interactions σ_e is decreased this effect should set in at smaller chain lengths. This is consistent with the simulation data: The data with the reduced interaction range show larger deviations at small chain lengths.

In the long chain length limit $\mathcal{N} \to \infty$, strictly symmetric blends in 3 spatial dimensions are very well describable by mean field theory, if the χ parameter is identified via the intermolecular pair correlation function of the athermal blend. The decoupling of composition and density fluctuations and the temperature independence of the structure of the underlying monomer fluid in the temperature range, where the phase separation in the binary blends occurs, give rise to a purely enthalpic χ parameter. For finite chain length, deviation between the MC results can be traced back to composition fluctuations. At the critical point, however, the mean field theory fails, and we observe 3D Ising critical behavior in accord with general arguments and deviations from mean field theory observed in simulation and experiment.

4.1.2 Films and Twodimensional Systems

Much of the success of the mean field description is related to the strong interdigitation of the polymers in the bulk. This quantity is measured by $\mathcal{N} = (\Phi R_e^d)^2$. It increases like the chain length N in $d = 3$ spatial dimensions. If the polymers are confined into quasi-twodimensional configurations the chain dimensions remain Gaussian ($R_e^2 \sim N$) in a dense melt. In this case, however, the quantity $\mathcal{N}$ is, to the leading order, independent from the chain length, i.e., a given molecule interacts only with a finite number of neighbors.

Let us consider a simple scaling argument for the behavior of the chain conformations upon confining a polymer into a thin film. According to Silverberg's argument[62] the chain conformations can be conceived simply as random walks reflected at the surface. If a finite stiffness (or bending rigidity) along the chain is considered, parallel and perpendicular chain dimensions are no longer independent, but this short-ranged correlation along the chain is not expected to affect the properties on long length scales.

At some film thickness D, however, the description of the polymer conformations as mutually non–interacting Gaussian chains will fail. When the film thickness becomes very small, the chain folds back many times into its own volume and the density inside of the Gaussian coil increases. The fractal structure of the segments of a single chain gradually becomes compact (i.e., space–filling). When the density inside of the coil finally becomes comparable to the average density of the melt, the parallel chain extension begins to grow

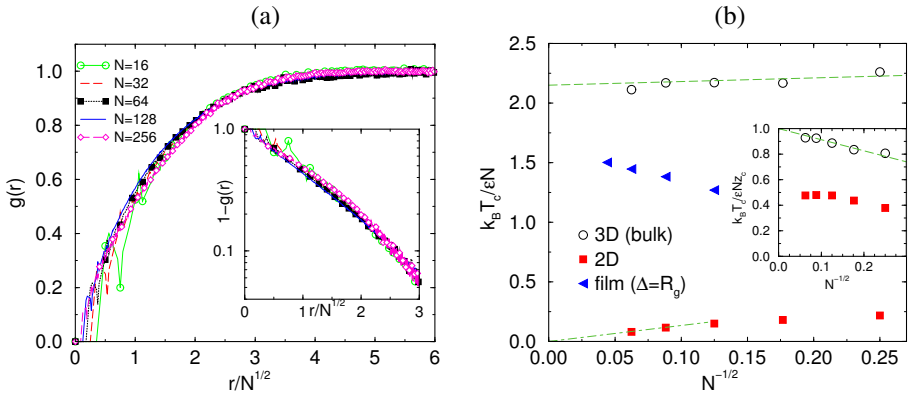

Figure 4. (**a**) Scaling plot of the intermolecular pair correlation function $g(r)$ versus $r/N^{1/2} \sim r/R$. Data are always taken close to criticality, but refer to all chains independent of their species. Chain lengths $N = 16, 32, 64, 128$, and 256 are included, as indicated in the key. For short chain lengths oscillations on the length scale of a few lattice units are visible and arise from packing effects. The inset shows $1 - g(r)$ on a logarithmic scale (cf. Eq.23) (**b**) Scaling of T_c/N and T_c/Nz_c (inset) *vs.* $N^{-1/2}$. For comparison the results for the 3d model are included. Adapted from Cavallo et al.[61].

such that the density of the film remains laterally homogeneous. In this limit the chains adopt disk–like compact conformations of polymers in two dimensions. The stretching parallel to the surface is only negligible when $\rho D R_e^2 \ll N$ or

$$\frac{D}{R_e} \gg \frac{1}{\sqrt{N}} \tag{22}$$

where R_e denotes the unperturbed chain extension in the bulk. This reasoning suggests the following behavior of the average chain conformation in a thin film: (**i**) For $D \gg R_e$ the chain extensions parallel and perpendicular to the surface are unperturbed. Here, we expect also the intermolecular paircorrelation function not to deviate strongly from the bulk behavior. (**ii**) For $R_e \gg D \gg R_e/\sqrt{N}$ the parallel chain extensions are unperturbed, but the chain folds back into the volume of its own coil. Other chains are gradually squeezed out of this volume, i.e., the correlation hole in the intermolecular paircorrelation function deepens and the interdigitation of the chains decreases. In this regime, the number of intermolecular contacts z_c is reduced, but it is still a finite number. (**iii**) For $R_e/\sqrt{N} \gg D$ the chains do not overlap strongly and stretch parallel to the surface as to maintain a laterally uniform density. The lateral extension scales like: $R_\parallel^2 \sim R_e^3/(D\sqrt{N})$. Note that this effect occurs, when the film thickness is of the order of the excluded volume screening length $\xi_{\rm ev} \sim R_e/\sqrt{N}$.[63] In this quasi-twodimensional limit, the correlation hole is describable by:

$$g^{\rm inter}(r) = 1 - c\ \exp\left(-\frac{\text{const}\cdot r}{R_e}\right) \qquad \text{for} \qquad r > \xi \tag{23}$$

where $c \leq 1$ is a constant. The exponential term corresponds to the correlation function of a Gaussian walk in two dimensions and the functional form suggests that the correlation hole in the intermolecular paircorrelation function in a dense melt is exactly canceled by the

density of the monomers of the reference chain, as it is the case in three dimensions. The MC data for the intermolecular paircorrelation function are presented in Fig. 4 (**a**). The data are compatible with the value $c = 1$. Therefore, the intermolecular paircorrelation function behaves at small distances like $1 - \exp(-\text{const} \cdot r/R_e) \approx \text{const} \cdot r/R_e)$ and the number of intermolecular contacts per monomer is proportional to $\rho g^{\text{inter}}(b) \sim 1/\sqrt{N}$. This implies a scaling of the critical temperature like $T_c \sim N z_c \sim \sqrt{N}$, as it is compatible with the simulation data shown in Fig. 4 (**b**). Indeed, T_c/N decreases like $N^{-1/2}$ as suggested by the scaling arguments. Unlike the situation in three spatial dimensions the mean field theory does not become quantitatively correct in the limit of long chain lengths. In two dimensions, even long chains interact only with a finite number of neighbors, and therefore $T_c/z_c N$ does not tend to unity for $N \to \infty$ (cf. inset of panel (**b**)).

Of course, these considerations highlight the influence of the confined chain conformations on the miscibility. If the surfaces prefer one component of the mixture, one encounters wetting transitions that might also lead to a pronounced alteration of the phase diagram in confined geometry.[64–66]

4.2 Entropic Contribution to the χ Parameter: Non-Additive Packing

The simple form of the χ parameter is based on the decoupling of density fluctuations or packing effects from molecular architecture, composition of the blend, and temperature. To illustrate the consequences of chain architecture on the miscibility behavior, let us discuss a further example: A blend of polymers with indented monomer shapes. In Fig.5 (**a**) we sketch a symmetric mixture with indented monomer shapes.[67] As one can observe, monomers of different types are separated by a spatial distance of at least $\sqrt{3}$, whereas monomers of the same species can approach each other up to a distance 2. The properties of the pure phases are not altered, because the packing constraints only restrict the minimal distance between unlike species. Of course, this extremely simple monomer shape is no faithful representation of realistic monomer packing effects on a microscopic length scale. However, in the spirit that a monomer in the bond fluctuation model corresponds to a small number of chemical repeat units, we expect the model to capture some universal, long-wavelength properties on the coarse–grained length scale of a Kuhnian segment. The shape of the monomers leads to a non-additive packing between monomers of different species. In an A-rich phase an A polymer possesses more conformational freedom as in a B–rich environment. Hence the free energy of mixing acquires also an entropic contribution.

We cannot resort to the simple estimate of the χ parameter (11), but we have to go back a step and approximate the partition function. Let us consider the ratio of the canonical partition functions of an additive mixture $\mathcal{Z}_{\text{add}}$ and a blend with non-additive monomer shape $\mathcal{Z}_{\text{nadd}}$:

$$\begin{aligned} \ln \frac{\mathcal{Z}_{\text{nadd}}}{\mathcal{Z}_{\text{add}}} &= \ln \frac{\sum \exp(-\beta E) \Pi_{i,j} (1 - \delta(r_{ij} - 2))}{\sum \exp(-\beta E)} \\ &= \ln \langle \Pi_{i,j} (1 - \delta(r_{ij} - 2)) \rangle_{|\text{add}} \end{aligned} \tag{24}$$

where the sum comprises all configurations of the additive mixture. The index i (j) runs through all monomers of type A (B) and the factor $(1 - \delta(r_{ij} - 2))$ excludes all configurations violating the non-additivity constraint. Neglecting correlations among the monomer positions, one can factorize the average and get to a first approximation:

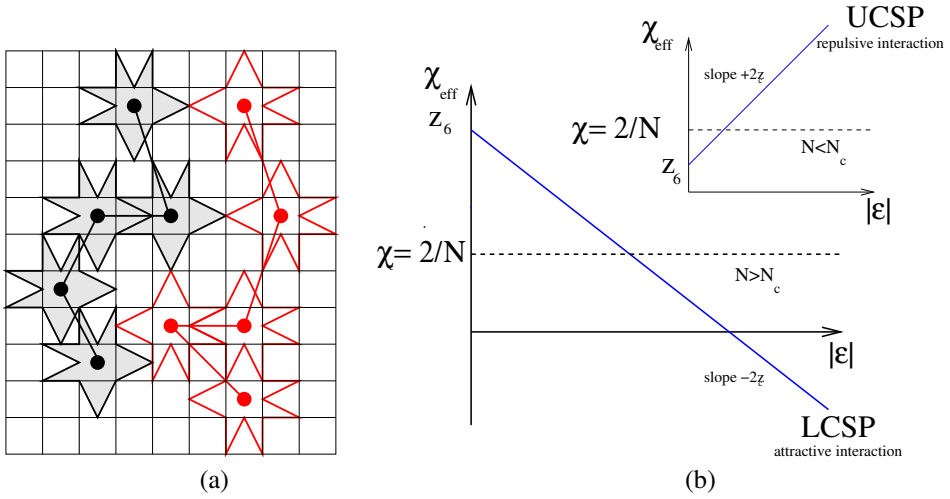

Figure 5. (**a**) Illustration of the intended monomer structure. A monomers are shaded, B monomers open. The effect of the indentation can be described by a non-additive hard core repulsion between monomers. As alluded, there is a strong entropic packing advantage which leads to phase separation. (**b**) Qualitative behavior of the χ-parameter for short chains (*UCSP*) and long chains (*LCSP*). From Müller.[67]

$$\begin{aligned}\ln \frac{\mathcal{Z}_{\text{nadd}}}{\mathcal{Z}_{\text{add}}} &\approx \sum_{i,j} \ln\langle(1-\delta(r_{ij}-2))\rangle_{|\text{add}} \\ &\approx -\sum_{i,j}\langle\delta(r_{ij}-2)\rangle_{|\text{add}} \\ &= -n_A n_B \frac{z_6}{V\Phi N} = -V\Phi N\phi(1-\phi)z_6 \end{aligned} \tag{25}$$

where z_6 corresponds to the mean number of particles at a distance 2 in an additive mixture. This quantity is accessible in the simulation via the intermolecular paircorrelation function in an additive mixture:

$$z_6 = \Phi N \sum_{i=1}^{6} g_{AB}(\boldsymbol{x}_i)|_{\text{add}} \tag{26}$$

where the pair correlation function is normalized such that $g(r) \to 1$ for $r \to \infty$. Neglecting all local packing effects, one gets $z_6 = 0.2625$. Finally the packing induced contribution to the free energy and the effective χ parameter takes the form:

$$\frac{\Delta V}{T\Phi V} \approx N z_6 \phi(1-\phi) \qquad \chi_{\text{eff}} = \chi_0 + z_6 = \frac{2z_c}{T} + z_6 \tag{27}$$

where z_c is the effective coordination number of the thermal interaction,i.e. the mean number of monomers of *other* chains within the range of the square well potential.[32] As anticipated the effective χ-parameter contains an enthalpic part and an entropic contribution. The excess entropy of mixing comprises two concurrent terms. The combinatorial

entropy stabilized the mixture whereas the packing contribution favors phase separation. Since the former is reduced by a factor $1/N$ the packing entropy dominates the behavior in the long chain limit.

The consequences for the miscibility behavior are discussed in Fig.5 (**b**): If the chain length is small enough, the translational entropy, which favors mixing dominates over the positive entropic contribution to the χ parameter. For $N < N_c \equiv 2/z_6$ the athermal blend is completely miscible. Upon lowering the temperature the blend phase separates at an upper critical solution temperature (UCST). For longer chains ($N > N_c$) the athermal blend is only partially miscible and to bring about a phase transition, we have to assume an attractive interaction between unlike species. Keeping with the notation of additive blends the attraction corresponds to negative values of ϵ. Upon increasing the absolute magnitude of the interactions $|\epsilon|$, the blend becomes miscible at a lower critical solution temperature (LCST):

$$\frac{1}{T_c} \sim -\epsilon_c = \frac{z_6}{2z_c}\left(1 - \frac{2}{z_6 N}\right) \tag{28}$$

The scaling of the lower critical solution temperature is in marked contrast to the scaling at the upper critical solution point with temperature. In the latter case the transition temperature is determined by a competition between the translational entropy of a polymer versus the monomeric repulsion; the critical temperature (UCST) increases linearly with chain length. In the former the conformational entropy per segment is balanced against the monomeric interactions and a chain length independent lower critical solution temperature (LCST) is approached from above. When expressed in terms of the χ parameter the Ginzburg criterion[57] and the critical amplitudes of the magnetization take the same form than for the upper critical solution points of the symmetric, additive mixture. However, when these quantities are written in terms of temperature the combination $(\chi_c - \chi)/\chi_c$ takes the form $Nz_c|T_c - T|/TT_c \approx 0.5Nz_6|T - T_c|/T$. This gives rise to an additional chain length dependence of the critical amplitudes and the Ginzburg number, when the temperature instead of the χ parameter is used in the vicinity of a lower critical solution point. For instance, the binodals in the temperature–composition plane open the wider the larger the chain length and the Ginzburg number which measures the relative distance between the critical temperature and the temperature where mean field behavior sets in becomes proportional to N^{-2}.

This mean field picture has been investigated via MC simulations[67] in the bond fluctuation model with the indented monomers sketched in Fig.5(**a**). Due to the additional excluded volume between unlike species the simulations have been performed at a reduced monomer density $\rho = 0.35/8$ in order to allow for a reasonable acceptance ratio of the semi-grandcanonical identity switches. Using a finite size scaling analysis we have determined the critical temperatures accurately. The dependence of the critical temperature on the chain length is summarized in Fig.6. For chain length $N = 10$ we find an upper critical solution temperature while for chain length $N = 16$ and larger we observe lower critical solution points. We find Ising critical behavior at the lower critical solution points and the temperatures approach a limiting value upon increasing the chain length. The critical temperatures are describable by a dependence of the form: $-\epsilon_c = 0.069(2) - 0.81(4)/N$. For chain length $N = 20$ we have measured $z_c = 1.41$ and $z_6 = 0.238$ in the MC simulations. This yields $\epsilon_c = 0.084 - 0.71/N$ as mean field estimate for the critical temperatures which

is also displayed in the Fig.6. It describes the simulation data only qualitatively. Deviations are partially due to the chain length dependence of the parameters z_c and z_6 via the correlation hole effect and composition fluctuations. Moreover, pronounced deviations stem from the crude approximation of the composition dependence of the the configurational entropy which lead to the simple expression(27). Our approximation treats the (rather strong) non additivity only perturbatively and neglects the composition dependence of the chain conformations (cf. Sec. 4.2.3).

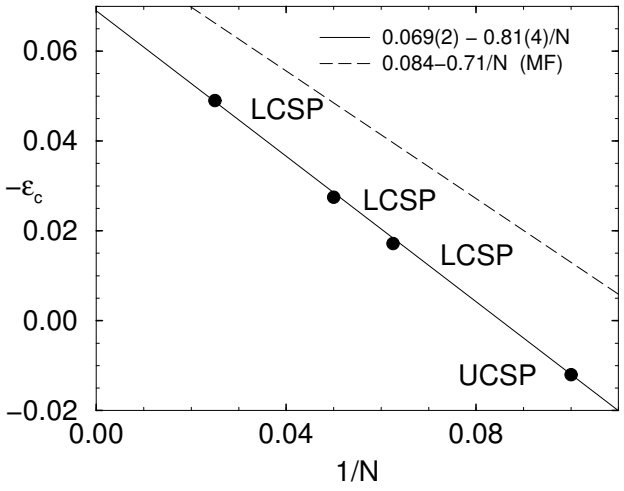

Figure 6. Chain length dependence of the critical temperature for mixtures of non-additive monomers. The straight line is given by $\epsilon_c = 0.069(2) - 0.81(4)\frac{1}{N}$. From Müller.[67].

If monomer of the same species pack less efficiently than monomers of the same species, a negative entropic contribution to the χ parameter results. An entropic contribution to the χ parameter occurs not only for non–additive monomer shapes but also for large enough disparities in the segment size. Mixtures of small and large spheres demix[68] when the size difference between the species is large enough. We expect the consequences to be even more pronounced for polymers due to the small entropy on mixing. These effects have been explored in the framework of the Lattice Cluster Theory.[13]

4.2.1 Entropic Contribution to χ Parameter: Stiffness Asymmetry

Generally, the constituents of a blend are not symmetric, and asymmetry might have pronounced effects on the miscibility behavior. Since the properties of a blend deviate from the linear superposition of the individual properties of its components, the blend has new, possibly favorable characteristics.

A common asymmetry in polymer blends are differences in the statistical segment length.[15] This effect has attracted much attention recently because of synthesis techniques for saturated hydrocarbon with a controlled degree of branching and their practical applications.[69] Bates[15] suggested that the degree of branching can be represented on a coarse–grained scale by a difference in statistical segment lengths. Graessley and co-workers[69] have studied systematically the miscibility behavior of this class of polymers. Many -

though not all blends – were describable in terms of Hildebrands solubility[70] parameters. This suggests that the incompatibility is chiefly determined by enthalpic effects.

In the framework of the bond fluctuation model the effect of stiffness can be incorporated via an intramolecular bond angle potential of the form:[71,67,25]

$$E(\theta) = f\cos(\theta) \tag{29}$$

where θ denotes the complementary angle to two successive bonds. Increasing the stiffness parameter f we energetically favor straight bond angles and increase the spatial extension of the molecule. The more open the molecule, the larger the number of intermolecular contacts. Upon increasing the stiffness parameter f from 0 (flexible chains) to 2 (semi-flexible), the chain extension for a polymer of $N = 32$ segments increases about a factor 1.5 and the number of intermolecular contacts z_c increases from 2.65 to 3.29 at $\epsilon = 0.05$ because the bond stiffness makes a folding back of the chain less probable.[67,25] Unfortunately, the behavior of the intermolecular paircorrelation function cannot be decomposed into packing effects of the monomeric units and polymeric correlation hole: On the one hand the chain structure is not Gaussian on all length scales, the rod-like behavior on short distances becomes more important upon increasing stiffness. On the other hand, the bond angle potential between neighboring monomers influences the packing structure of the liquid, which for semi-flexible chains differs from the packing of the monomer fluid. The interplay between the packing arrangement of the monomers and the local conformations favored by the bond angle potential gives rise to an entropic contribution to the Flory-Huggins parameter.

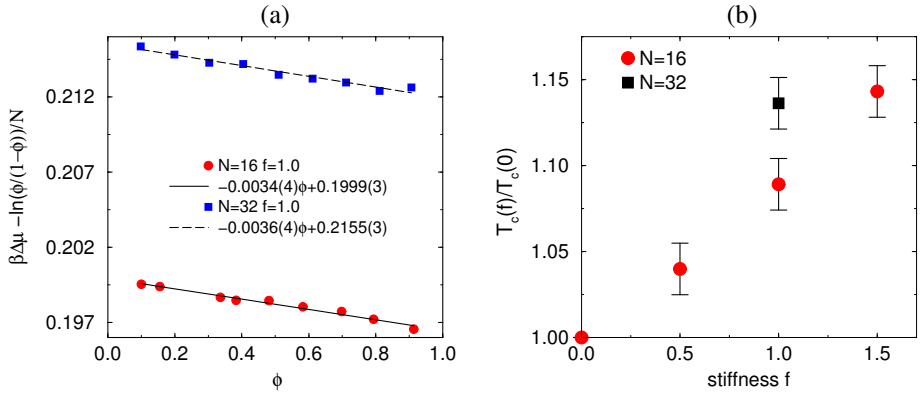

Figure 7. (**a**) Deviations from the semi-grandcanonical equation of state for blends of polymers with different stiffness. The (negative) slope is proportional to the entropic contribution to the χ parameter. (**b**) Dependence of the critical temperature on the stiffness f for chain length $N = 16$ and 32. From Müller.[67].

To explore the possibility of entropic contributions to the χ parameter,[67] we accurately measure the dependence of the chemical exchange potential $\Delta\mu$ per polymer on the composition of the mixture. If there were no entropic contributions to the χ parameter, only the (exactly known) translational entropy would determine the relation between the

exchange chemical potential $\delta\mu$ and the composition ϕ. In Fig.7 (**a**) we present the deviations $\beta\Delta\mu - \ln[\phi/(1-\phi)]$ from the ideal mixing behavior. An entropic contribution to χ is related to a composition dependence in the form $-\chi N(2\phi - 1)$. Indeed, the MC results do reveal a composition dependence of this form and we accurately extract a small positive entropic contribution $\Delta\chi$ to the Flory-Huggins parameter.[67] $\Delta\chi = 0.0017(2)$ for $N = 16$ and $f = 1$, $\Delta\chi = 0.0018(2)$ for $N = 32$ and $f = 1$, and $\Delta\chi = 0.0031(3)$ for $N = 16$ and $f = 1.5$. For the parameters investigated, the entropic contribution $\Delta\chi$ increases with stiffness disparity in the blend and is roughly independent of chain length. For the chain lengths considered, it is only a few per cent of the critical value $\chi_c = 2/N$ and we anticipate only a small increase in the critical temperature. If the chain length independence of the entropic contributions remains true in the long chain length limit, the data suggest that for long macromolecules ($N \approx \mathcal{O}(1000)$) the stiffness disparity alone will be sufficient to cause phase separation or LCST behavior.[67] The positive entropic contribution to the χ parameter is consistent with field theoretical studies by Liu, Fredrickson and Bates,[72] recent P-RISM calculations by Singh and Schweizer[73] and Lattice Cluster Theory by Foreman and Freed.[74]

Unfortunately, the semi-grandcanonical MC moves rapidly become less efficient as the chain length or the stiffness disparity is increased, because the typical conformations of the two species differ strongly. For the chain lengths accessible in the simulations the shift in the critical temperature is small and not chiefly determined by the entropic contribution to the χ parameter. Most notably, the stiffness increases the size of the molecules and the number of intermolecular contacts. Hence, the enthalpic contribution to the χ parameter increases as well. The increase of the enthalpic and entropic contributions are both of the order of a few percent. We expect both effects to persist in the long chain length limit.

For the short chain length considered in the simulation the mean field theory overestimates the critical temperature by about 20%. According to the Ginzburg criterion the deviation between the critical temperature and the mean field estimate decreases with the chain extension (cf. Eq.(21)). We expect composition fluctuations to shift the critical temperature down the less the higher stiffness. Even if the χ parameter remained unaltered, the critical temperature in the MC simulations (for short chains) would increase.

The measured shift of the critical temperature is presented in Fig.7 (**b**). Upon increasing the stiffness or the chain length the ratio of critical temperatures between the strictly symmetric blend and the blend with stiffness disparity increases. For $N = 16$ and $f = 1$ we obtain a relative shift of 9% for T_c. The entropic contribution in the athermal system amounts to $2\Delta\chi/N = 0.014$ while the relative increase of the effective coordination number is 6% as measured in the MC simulations. The remaining deviation is consistent with the dependence of the ratio T_c^{MF}/T_c on chain extension.

A similar study on the consequences of stiffness disparity was pursued in an off-lattice model by Weinhold et al.[75] Using the increment chemical potential method[37] the authors explored the miscibility behavior. Upon blending the chemical potential of the flexible chains increases, while the stiffer component lowers its free energy. This effect was rationalized via equation of state effects: At constant density the blend has a higher osmotic pressure than the pure flexible component and a lower osmotic pressure than the stiff component. The authors stated that the behavior is in almost quantitative agreement[75] to the simulations in the bond fluctuation model. Again this indicates that the lattice structure in the bond fluctuation model is a good approximation for the continuum space proper-

ties. The net excess free energy per monomer obtained from the simulations is essentially zero to within the $\pm 0.005T$ statistical error.[75] This is consistent with the small values $\Delta\chi$ found in our simulations. They also illustrated the significance of the intermolecular pair correlation function for the χ parameter.[76]

Structural asymmetries can lead also to a composition dependence of the Flory-Huggins parameter χ. Dudowicz et al[77] studied a dependence of the form: $\chi = a + (b + c\phi)/T$. Depending on the coefficients a,b, and c different phase behaviors can be observed, and the coefficients can be approximatively related to the structure of the monomeric units via the Lattice Cluster Theory.

4.2.2 Effects of Pressure or Solvent Density

The effect of pressure on the miscibility behavior has attracted much interest. There is an interesting interplay between equation of state effects and the phase behavior. This has also a practical importance when a blend is mixed in an extruder or during injection molding of plastics.[78] In the framework of the bond fluctuation model the local fluid structure is mainly determined by athermal packing effects. In the athermal melt, the osmotic pressure is independent of the chain length.[79] This chain length independence of the pressure at high densities is a universal property of polymer melts.[26] The excess free energy change upon mixing per monomer is of the order $\chi \sim 1/N$. The free energy cost for a density fluctuation (on the length scale of a monomer) is proportional to the compressibility and, hence, chain length independent. Therefore, in the one phase region, the interactions lead only to a small excess volume change upon mixing for high molecular weight (compatible) polymer blends. These kind of compressibility effects have been observed, e.g., at polymer–polymer interfaces, where the energetic unfavorable interactions at the interface result in a slight decrease of the density. However, even for rather strongly segregated blends[41] ($\chi N < 20$) in the bond fluctuation model the effect yields only a density reduction by a few percent. This is also in agreement with the decoupling of composition and density fluctuations. The insignificance of compressibility effects in weakly interacting blends and the consequences for the analysis of neutron scattering data has been explored in ref.[80,81] Gromov and de Pablo[82] found in MC simulations of a model of Lennard-Jones chains of length $N = 16$ a volume change of approximately 10% at constant pressure.

For our specific choice of interactions the total energy density per monomer is also of the order χ. Hence, the fluid structure corresponds to that of an athermal melt in the limit of long chain lengths and χN =const. This observation is in accord with the temperature independence of the packing and the effective coordination number in the temperature range where the phase separation occurs. If we were to simulate at constant pressure, the density around the phase transition would be chiefly determined by the value of the athermal system in the limit of long chains. Therefore, we expect not much change in the chain length dependence of the miscibility at constant volume or at constant pressure.

However, we would like to emphasize that the approximate decoupling between the fluid structure/density and the temperature (at constant pressure) is not a universal property and does depend on the specific choice of the interactions. Unlike the excess free energy change upon mixing, the total energy density per monomer needs not to be small for long polymers at χN =const. In many experimental instances, concentrated polymer solutions and melts exhibit a temperature dependent equation of state. Therefore the

density Φ is a function of temperature T at a given fixed pressure. If the Flory-Huggins parameter χ is mainly enthalpic, we still can use Eq.(11) to calculate the χ parameter. In a very crude approximation the intermolecular pair correlation function is independent of the density. Then the effective coordination number is proportional to the monomer density $\rho = \Phi N$. The critical temperature of the blend at constant pressure scales like $T_c \sim \rho(T_c)N$. For a blend with an UCSP the critical temperature increases with chain length and the monomer density $\rho(T_c)$ at the critical temperature decreases. This leads to a weaker dependence of the critical temperature with chain length. Such an effect has been observed in various experiments. Escobedo and de Pablo[60] have investigated the scaling of the critical temperature in a symmetric blend under constant pressure. They found that the critical temperature increases effectively like $\sqrt{N}$ for the range of chain length investigated. Moreover, recent experiments on polyolefin blends by Lohse and co-workers find evidence for a temperature-pressure superposition:[78] Far from the UCST the interaction energies depend on the pressure P only via $\rho(P)$. However, deviations from this scaling are found for blends which demix upon heating. This might indicate an additional dependence of the local packing arrangements with the density.

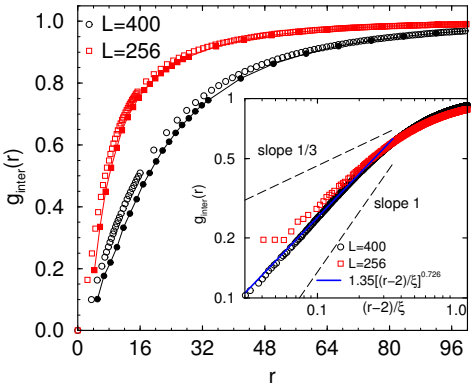

Figure 8. Real space dependence of the intermolecular correlations: (**a**) Intermolecular pair correlation function $g^{\rm inter}(r)$ for chain length $N = 2048$ and monomer number densities $\rho = 0.0032$ (L=400) and $\rho = 0.0122$ (L= 256). Open symbols correspond to the MC results, whereas filled one represent the RG calculations. Inset: Power-law dependence of $g^{\rm inter}(\mathbf{r})$ at small distance. The data are compatible with a dependence of the form $g^{\rm inter}(\mathbf{r}) \sim r^{\alpha}$ with an exponent $0.7(3)$, close to the predicted value $\alpha = 0.8$. From Müller et al.[83]

If the density becomes lower one obtains a semi-dilute solution instead of a melt: In a 3-dimensional melt the chain statistics is Gaussian up to microscopic length scales and the correlation hole in the intermolecular pair correlation function has only a finite depth. In a semi-dilute solution, the chain statistics is Gaussian for distances larger than the excluded volume screening length $\xi_{\rm ev}$, but self-avoiding walk-like for smaller distances, i.e., inside the excluded volume blob. The size of the excluded volume blob $\xi_{\rm ev}$ can be determined by requiring that the monomer density inside the blob is mainly created by monomers of the same chain. Let g denote the number of monomeric units inside the blob, then $\rho = g/b_{\rm ev}^3 g^{3\nu_{\rm ev}}$, where $\nu_{\rm ev} = 0.588$ characterizes the chain extension of a self-avoiding walk $R \sim b_{\rm ev} N^{\nu_{\rm ev}}$. Therefore the size of the blob decreases with density like $\xi \sim b_{\rm ev}(\rho b_{\rm ev}^3)^{-\nu_{\rm ev}/(3\nu_{\rm ev}-1)}$. Thus, the number of monomers of other chains inside the excluded volume blob is small and chains do not interdigitate on the length scale $\xi_{\rm ev}$ or smaller. The intermolecular paircorrelation function exhibits a deep correlation hole and shows a power-law behavior $g^{\rm inter}(\mathbf{r}) \sim (r/\xi_{\rm ev})^{\alpha}$ for $r < \xi_{\rm ev}$ (cf. Fig. 8). The exponent adopts the value $\alpha = 3 - 2/\nu_{\rm ev} - \omega_{12} \approx 0.8$,[83,84] where $\omega_{12} \approx 0.4$ is the

correction to scaling exponent that characterizes the contacts ($\sim N^{\nu\omega_{12}}$) of two mutually interdigitating self-avoiding walks. The number of intermolecular contacts scales like $\chi \sim z_c \sim \rho g^{\text{inter}}(\sigma_e) \sim (\rho b_{\text{ev}}^3)^{(1+\nu\omega_{12})/(3\nu_{\text{ev}}-1)} \sim \rho^{0.616}$. This effect – the Joanny renormalization of the Flory-Huggins parameter – has been worked out in detail by Leibler[85] and Schäfer.[86]

If the two components differ strongly in their equation of state, more complex phase diagrams occur (cf. Konynenburg and Scott[5] for a classification of possible types of miscibility behavior in compressible blends). In addition to liquid-liquid phase separation one encounters liquid-vapor phase coexistence and three phase coexistence regions where two liquids and a vapor phase coexist.

4.2.3 Single Chain Conformations.

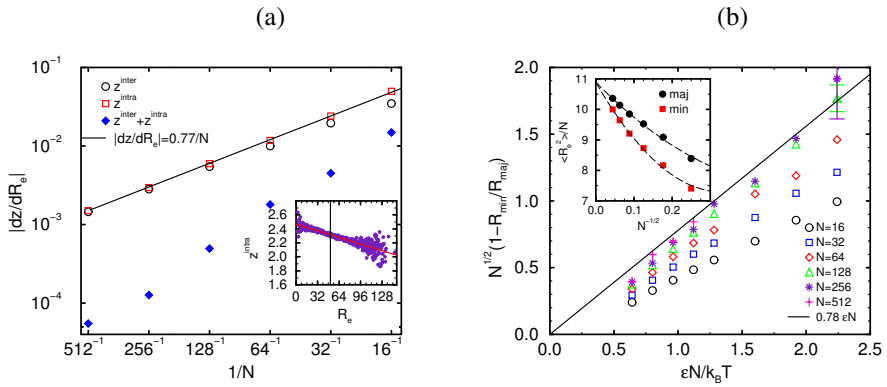

Figure 9. (**a**) Correlation between the chain extension and the number of intermolecular and intramolecular contacts. The straight line marks the prediction of the scaling considerations $\mathrm{d}z/\mathrm{d}R \sim 1/N$. (**b**) Shrinking of the end-to-end extension below the critical temperature. The solid line marks the expected behavior for long chain lengths. The inset in (**a**) shows the chain length dependence of end-to-end distance of the majority and minority component at constant $\epsilon N = 0.64$. Lines in the inset are only guides to the eye. From Müller.[22]

Sophisticated theoretical approaches have been developed to study the dependence of chain conformations on the environment: self-consistent P-RISM theory[87,88], SCF theory for clusters of chains[22], and ellipsoid models.[20,89] In the following we constrain ourselves to MC simulations and simple scaling arguments.

MC simulations suggest that one possible mechanism of conformational changes in blends is associated with exchanging energetically unfavorable intermolecular contacts for attractive intramolecular contacts upon reducing the spatial extension of the molecule. Attributing this shrinking of the minority component to a balance between the entropy loss due to deviations from the unperturbed conformations and energy gain upon shrinking, we can estimate the magnitude of conformational changes:[22] Within the Gaussian chain model a deviation from the unperturbed chain extension R_e gives rise to an entropic force of the form

$$\frac{\mathrm{d}S}{\mathrm{d}R} \sim \frac{(R - R_e)}{R_e^2} \tag{30}$$

This is opposed to an enthalpic force $\mathrm{d}E/\mathrm{d}R$, where E denotes the single chain energy. E comprises energetically favorable interactions Nz^{intra} among monomers of the same chain and Nz^{inter} interactions with monomers of other polymers. The exchange of an intermolecular interaction with an intramolecular one lowers the single chain energy by an amount of the order χ. The number of intramolecular interactions per monomer z^{intra} is given by the density of monomers of the same chain inside of its volume $z^{\mathrm{intra}} \sim 1/\Phi R_e^3 \sim 1/\sqrt{\mathcal{N}}$. Under the assumption that the reduction of the chain extension does not affect the total number of interactions, but merely exchanges intermolecular interactions into energetically favorable intramolecular ones, we estimate the chain length dependence of the energy change as

$$\frac{\mathrm{d}E}{\mathrm{d}R} \sim -\frac{\chi N}{\Phi R_e^4}. \tag{31}$$

Balancing the entropic force against the enthalpic one, we obtain:

$$\frac{R_e - R}{R_e} \sim \frac{\chi N}{\Phi R_e^3} = \frac{\chi N}{\sqrt{\mathcal{N}}}. \tag{32}$$

These scaling arguments are similar to those for a chain in a marginal solvent and suggest that the perturbation of the chain conformations decreases upon increasing the chain length at $\chi N = \mathrm{const}$. The conformations in high molecular weight blends are only very mildly perturbed in the minority phase.

The derivation of the scaling arguments relies on the number of intramolecular contacts and its dependence of the chain extension. Obviously, this estimate excludes contributions from the neighbors along the polymer, which give rise to $z^{\mathrm{intra}} \sim N$. Though the neighbor contribution is important for the scaling of the number of intramolecular contacts with chain length, we assume them to be independent from the instantaneous shape/extension of the polymer. [a]

Using the scaling estimate above, the dependence of the z^{intra} on the instantaneous extension R at fixed chain length is given by: $\mathrm{d}z^{\mathrm{intra}}/\mathrm{d}R \sim 1/\Phi R_e^4 \sim 1/N$. Clearly, a detailed verification of this scaling behavior by MC simulations is warranted. Such a test is presented in Fig.9 (**a**). The inset presents the average number of intramolecular contacts at fixed end-to-end distance for an athermal melt of chain length $N = 256$. At the mean end-to-end distance $\sqrt{\langle R^2 \rangle_0}$ we determine the slope $\mathrm{d}z/\mathrm{d}R$ as indicated by linear regression. The chain length dependence of the derivatives of the number of inter- and intramolecular contacts with respect to the chain extension decreases like $1/N$ for large chain lengths. This confirms the scaling predictions. Moreover, the sum of intermolecular and intramolecular contacts depends much weaker on the spatial extension R_e and the dependence decreases faster than $1/N$. This indicates that the fluid structure of the monomers is mainly determined by packing and approximately decouples from the chain conformations. For long chains, the conformational changes merely result in an exchange of inter- and intramolecular contacts. From the MC data we estimate $\mathrm{dz/dR} = 0.77(7)/N$ for the bond fluctuation model at density $\rho \equiv \Phi N = 1/16$.

The scaling predictions can be made more quantitatively in the framework of the Gaussian chain model. Let $P(\mathbf{R})$ denote the probability distribution of the end-to-end vector $\mathbf{R}$ which incorporates the dependence of the single chain energy E on the chain extension.

[a] The fact that the number of intermolecular contacts per chain Nz^{intra} scales with N, but its derivative with

$$E(\mathbf{R}) \approx E(\sqrt{\langle R_e^2\rangle_0}) + \frac{\mathrm{d}E}{\mathrm{d}R}\left[|\mathbf{R}| - \sqrt{\langle R_e^2\rangle_0}\right] \tag{33}$$

where $\langle R_e^2\rangle_0 = b^2N$ denotes the end-to-end distance in the athermal limit. Assuming Gaussian statistics for the unperturbed chain, we can write the probability distribution for a B polymer in the form

$$P(\mathbf{R}) \sim \exp\left(-\frac{3\mathbf{R}^2}{2\langle R_e^2\rangle_0} - \frac{1}{T}\frac{\mathrm{d}E}{\mathrm{d}R}\left[|\mathbf{R}| - \sqrt{\langle R_e^2\rangle_0}\right]\right). \tag{34}$$

The total energy change associated with the transfer of two intermolecular contacts of a B polymer $[\epsilon(2\langle\phi\rangle - 1)]$ into an intermolecular contact $[-\epsilon]$ and a contact between monomers not belonging to this B polymer $[-\epsilon(2\langle\phi\rangle - 1)^2]$ amounts to $\Delta E = 4\epsilon\langle\phi\rangle^2$. The number of intramolecular contacts per monomer increases by 2, and the number of intermolecular contacts decreases by the same amount. Therefore $\mathrm{d}E/\mathrm{d}R$ equals $2\epsilon\langle\phi\rangle^2\mathrm{d}z/\mathrm{d}R$. Using this estimate and assuming that the conformational changes are small, we calculate the mean square end-to-end distance:

$$\langle R_e^2\rangle \approx \langle R_e^2\rangle_0\left(1 - \sqrt{\frac{8}{27\pi}}\frac{1}{\sqrt{\mathcal{N}}}\left[\frac{\Phi R_e^4}{z_c}\frac{\mathrm{d}z^{\mathrm{intra}}}{\mathrm{d}R}\right]\chi N\langle\phi\rangle^2\right) \tag{35}$$

We expect this asymptotic expression to hold only for very small values of $\chi N/\sqrt{\mathcal{N}}$, where the conformational changes can be treated perturbatively. This expression predicts a quadratic dependence of the chain extension on the composition of the mixture. The effect

---

respect to the chain dimension R is independent of the chain length can be rationalized in the framework of the Gaussian chain model. Let $R_0^2 = bN^2$ denote the unperturbed end-to-end distance. For convenience, we replace the square well contacts by Gaussian contacts of widths σ_e. Then, the number of intramolecular contacts can be written in the form:

$$Nz^{\mathrm{intra}}(R) \sim \frac{1}{2}\int \mathrm{d}s\ \mathrm{d}s'\ \mathrm{d}^3\xi \left(\frac{3}{2\pi\sigma_e^2}\right)^{3/2}\left(\frac{3}{2\pi b^2|s-s'|}\right)^{3/2}\left(\frac{3}{2\pi b^2(N-|s-s'|)}\right)^{3/2}\left(\frac{3}{2\pi b^2 N}\right)^{-3/2}$$
$$\exp\left(-\frac{3\xi^2}{2\sigma_e^2}\right)\exp\left(-\frac{3\xi^2}{2b^2|s-s'|}\right)\exp\left(-\frac{3(R-\xi)^2}{2b^2(N-|s-s'|)}\right)\exp\left(+\frac{3R^2}{2b^2N}\right)$$

In the limit $\sigma_e \ll b^2N$ this expression can be simplified to:

$$Nz^{\mathrm{intra}}(R) \sim \int_0^N \mathrm{d}\triangle s\ (N-\triangle s)\left(\frac{3}{2\pi(\sigma_e^2 + b^2\triangle s)}\right)^{3/2}\left(\frac{N}{N-\triangle s}\right)^{3/2}$$
$$\exp\left(-\frac{3R^2}{2b^2N}\ \frac{\triangle s}{N-\triangle s}\right)$$

The major contribution to this integral comes from $\triangle s \approx 0$, i.e., the neighbors along the chain dominate the number of intramolecular contacts. Nz^{intra} scales like N. The derivative with respect to R is given by:

$$\frac{\mathrm{d}Nz^{\mathrm{intra}}}{\mathrm{d}R} \sim \int_0^N \mathrm{d}\triangle s\ (N-\triangle s)\left(\frac{3}{2\pi(\sigma_e^2 + b^2\triangle s)}\right)^{3/2}\left(\frac{N}{N-\triangle s}\right)^{3/2}$$
$$\frac{3R}{b^2N}\frac{\triangle s}{N-\triangle s}\exp\left(-\frac{3R^2}{2b^2N}\ \frac{\triangle s}{N-\triangle s}\right)$$

The integral converges in the limit $\sigma_e \to 0$ and scales like N^0 at $R = R_0$.

increases linearly with the χ parameter, but decreases at fixed χN like $1/\sqrt{\mathcal{N}}$. Hence, the conformations of long macromolecules are only very weakly dependent on composition. This is also in qualitative agreement with field theoretical calculations of Vilgis and Holyst,[90] and Garas and Kosmas.[91] A decreasing dependence of the single chain conformations on the environment is also found in simulations and self-consistent P-RISM calculations for atomistic models[21].

In Fig.9(**b**) we explore the scaling of the shrinking of the chains in the minority phase at two phase coexistence. The simple estimate (35) predicts that the chains in the majority phase are unperturbed, while the minority component reduces its size in a well segregated blend. The relative shrinking $1 - R_{\min}/R_{\mathrm{maj}}$ increases linearly with ϵN and is at fixed ϵN of the order $1/\sqrt{\mathcal{N}}$. This is in qualitative agreement with the simulation data for the end-to-end distance presented in Fig.9(**b**). The straight line represents the prediction of Eq.(35). Surprisingly, the simulation data approach the asymptotic behavior very slowly. Only for chain length $N \geq 128$ the simulations reach the scaling limit; for smaller chain length the estimate (35) overpredicts the shrinking.

There are at least two possible reasons for the pronounced small chain length corrections to the scaling behavior: First, the considerations hold only in the regime $2 \ll \chi N \ll \sqrt{\mathcal{N}}$. The first limit is set by the condition that the blend is well segregated, i.e., $\langle\phi\rangle_{\min} \ll 1$. The second requirement corresponds to small conformational changes. This temperature regime is experimentally relevant because the concentration of the minority component is small but does not vanish for long chain lengths. However, for short chain lengths these conditions are rather restrictive. For very strong segregation the linear decrease of the chain dimensions with $\chi N/\sqrt{\mathcal{N}}$ will certainly break down and the changes cannot be treated perturbatively.

A second source of corrections to asymptotic scaling behavior might be deviations from the Gaussian chain statistics upon shrinking. The ratio between the end-to-end distance and the radius of a completely collapsed coil $(3/4\pi b^3\rho\sqrt{N})^{1/3} = (3/4\pi\sqrt{\mathcal{N}})^{1/3}$ decreases only very weakly with chain length. Even for the chain length $N = 256$ the end-to-end distance exceeds the radius of the densely packed coil only by a factor of 5. If the extension of the shrunken chain becomes comparable to the size of the completely collapsed coil, it cannot reduce its size much further. In this case the data would not scale as a function of $\chi N/\sqrt{\mathcal{N}}$, but they would crossover to a temperature independent end-to-end distance the earlier the smaller the chain length.

The conformational changes result in a composition dependence of the segmental entropies and, hence, give rise to a composition dependence of the χ parameter. The scaling arguments suggest that the conformational changes alone might only produce an effect of the order $1/N$ per chain. Using the relation between the exchange chemical potential and the composition we can measure a χ parameter. In the one phase region far above the critical temperature we observe an upward parabolic dependence of the χ parameter on the composition. The composition dependence is about 4%.

4.3 Interfaces

A symmetric binary blend will partition into two coexisting phases already at high temperatures. Domains of the two phases will form and they will be are separated by interfaces. Comparing the properties of interfaces as obtained from simulations or experiments to the

predictions of mean field theory one has to distinguish two types of properties: Excess quantities which do not make any explicit reference to the interface position - like e.g., the interface tension or the surface excess of a component - can be directly compared. Profiles across the interfaces or observables that depend on the local position of the interfaces are affected by capillary waves.

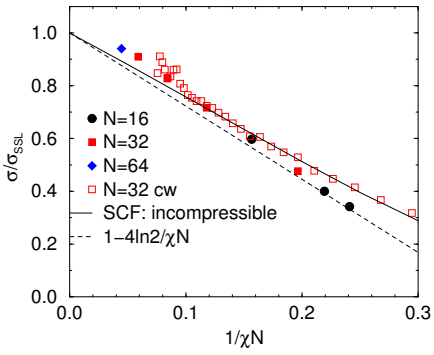

Figure 10. Interface tension in units of $\sigma_{\rm SSL} R_e^2/T = \sqrt{\mathcal{N}}\sqrt{\chi N/6}$. The symbols correspond to MC simulations for three chain length as indicated in the key. The interfacial tension has been extracted from the probability distribution of the composition in the semi-grandcanonical ensemble, and the spectrum of capillary waves (for $N = 32$). Data are compared to SCF results and the exact asymptotic correction in the limit $\chi N \to \infty$ by Semenov.[92] Adapted from Schmid and Müller.[93]

In Fig.10 we compare the interface tension extracted from the simulations to the prediction of the SCF theory using the identification of the Flory-Huggins parameter χ as in the previous section. The simulation data confirm, that σ/σ_{SSL} is only a function of χN and they agree quantitatively with the SCF theory.

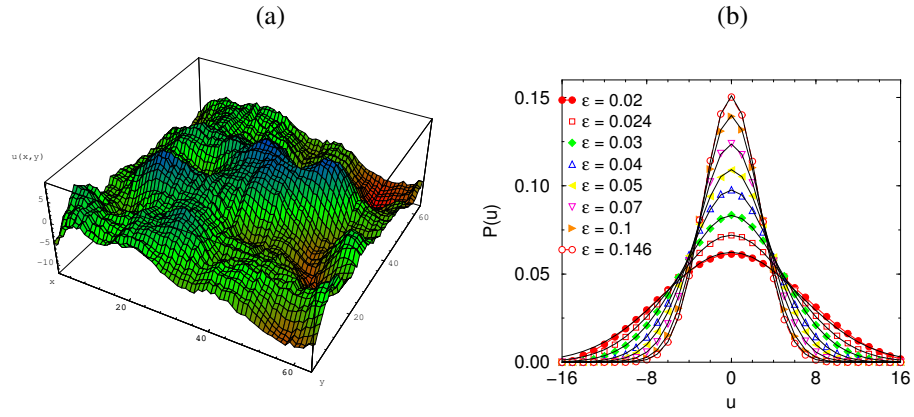

Figure 11. (**a**) Fluctuations of the local interface position in a binary polymer blend at $\epsilon = 0.03$ ($\chi N \approx 5.1$). The position has been averaged over a lateral size of $B = 8$. (**b**) Distribution of the local interface positions as a function of the incompatibility ϵ. From Werner et al.[94]

A comparison of profiles between simulations/experiments and SCF calculations has to take due account of the fluctuations of the local interface position. Interfaces are not perfectly flat, as assumed in the SCF calculations, but there are thermal fluctuations. A snapshot of the interface position in the MC simulations of a binary blend is shown in

Fig.11(**a**). To a first approximation the effect of these fluctuations is to increase the effective area of the interface. Let $u(\mathbf{r}\|)$ denote the local interface position. Then, the free energy cost of deviations from perfectly flat configurations are described by the Hamiltonian $\mathcal{H}$:

$$\mathcal{H}[u(\mathbf{r}_\|)] = \int \mathrm{d}^2\mathbf{r}_\| \ \left\{ \frac{\sigma}{2}|\nabla u|^2 + \frac{\kappa}{2}|\triangle u|^2 \right\} \tag{36}$$

This is an expansion in terms of small u and its derivatives, σ denotes the interfacial tension and κ the bending rigidity. For interfaces between not too long homopolymers κ is very small; for copolymer loaden interfaces, however, the second term becomes important as we shall discuss. This capillary wave Hamiltonian is diagonal and quadratic in terms of the Fourier components $u(q)$ and the equipartition theorem yields for the spectrum of fluctuations in thermal equilibrium:

$$\langle u^2(q)\rangle = \frac{T}{\sigma q^2 + \kappa q^4} \tag{37}$$

The local positions $u(\mathbf{r}_\|)$ are also Gaussian distributed $P(u)$ with variance s:

$$s^2 = \frac{1}{4\pi^2}\int \mathrm{d}^2\mathbf{q}_\| \langle u^2(\mathbf{q}_\|)\rangle = \frac{T}{2\pi\sigma}\ln\left(\frac{q_{\max}}{q_{\min}}\right) \tag{38}$$

where a short and long length scale cut–off $q_{\max}$ and $q_{\min}$ have to be introduced to avoid the divergence at $q \to 0$ and $q \to \infty$. The bending rigidity κ has been neglected, it would make the cut–off at small distance obsolete. The MC result for the distribution $P(u)$ of the local positions is presented in Fig.11(**b**). Upon decreasing the incompatibility ϵ, we increase the strength of the fluctuations.

These capillary waves broaden the apparent profiles p_{app}. Laterally averaged profiles, as obtained in experiments or MC simulations, are describable via the convolution of an intrinsic profiles p_{int} of an ideally flat interfaces and the distribution of the local positions

$$p_{\mathrm{app}}(z) = \int \mathrm{d}u \ P(u) p_{\mathrm{int}}(z-u) \ , \tag{39}$$

where z denotes the coordinate perpendicular. When applied to a erfc-shape profile, one obtains:[95,94,96]

$$\frac{w_{\mathrm{app}}^2}{R_e^2} = \frac{w_{\mathrm{int}}^2}{R_e^2} + \frac{T}{4\sigma R_e^2}\ln\left(\frac{q_{\max}}{q_{\min}}\right) \tag{40}$$

$$\overset{\chi N \gg 2}{=} \frac{1}{\sqrt{6\chi N}}\left(1 + \frac{3}{2\sqrt{\mathcal{N}}}\ln\frac{q_{\max}}{q_{\min}}\right) \tag{41}$$

where we have used the expression for the strong segregation limit in the last line. The apparent width is broader than the intrinsic one and depends via the two cut-offs on the system geometry.[95,94] For a free interface the lower cut–off $q_{\min}$ is set by the lateral block size B on which the interface is observed. This might be set by the size of the simulation cell or the coherence length of the neutron beam by which the interfacial structure is investigated. Gravitation or interactions with walls/surfaces also limit long-wavelength

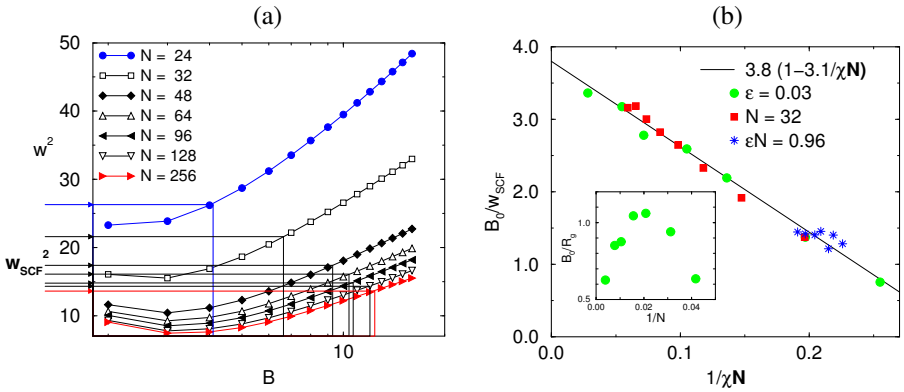

Figure 12. (**a**) Dependence of the apparent interfacial width on the lateral block size B at constant incompatibility $\epsilon = 0.03$ for different chain lengths. From the intersections of the simulation data with the SCF predictions (presented as horizontal lines) we determine the small length scale cut–off B_0. (**b**) The ratio $B_0/w_{\rm scf}$ approaches a constant value 3.8. Leading corrections are of the order $1/\chi N$. Note that data sets at constant N, χN and χ collapse in this representation. The inset shows the ratio B_0/R_e for fixed incompatibility $\epsilon = 0.03$. The ratio tends to zero for large N. From Werner et al.[94]

fluctuations. The upper cut-off $q_{\rm max}$ describes the crossover from capillary waves (on large distances) to "intrinsic" fluctuations, which build up the smooth profile of the ideally flat interface. Measuring the width of an interface in the experiments or simulations one cannot extract both, the "intrinsic" width $w_{\rm int}$ and the upper cut-off $q_{\rm max}$ individually.

Polymer blends are well suited to examine this crossover, because the strong interdigitation of the molecules makes SCF calculations describe the properties of interfaces accurately except for capillary wave fluctuations. Taking the SCF prediction as the "intrinsic" width of an hypothetical flat interface, we use Eq. (40) to *define* the length scale $B_0 = 2\pi/q_{\rm max}$ at which the crossover between "intrinsic" fluctuations and capillary waves occurs. This procedure is illustrated in Fig.12(**a**). There are three possible candidates for B_0: A microscopic length scale (e.g., the bond length) independent from temperature or chain length; the width of the interface, which depends on temperature but not on N; or the radius of gyration/correlation length which depends both on χN and R_e. The simulation data[94] in panel (**b**) indicate a behavior of the form $B_0 = 3.8 w_{\rm scf}(1 - 3.1/\chi N)$, i.e. the intrinsic width of the interface sets the crossover length; a result compatible with calculations of Semenov.[97]

The spectrum of interfacial fluctuations is an alternative route for measuring the interfacial tension in MC simulations. This is illustrated for a blend with a structural asymmetry in Fig.13. When we increase the stiffness disparity, the semi-grandcanonical identity switches become increasingly inefficient and σ cannot be obtained via pre-weighting techniques. Stiffness increases the incompatibility and this, in turn, results in a larger interfacial tension (c.f. Fig.13(**a**)). This effect is quantitatively captured by the SCF calculations which account for the detailed chain architecture. Qualitative agreement is also obtained within the Gaussian chain model. The deviations from the prediction of Helfand and Sapse[98] are mainly due to chain end corrections. The situation is qualitatively different for the intrinsic width of the interface (c.f. panel (**b**)). MC simulations and SCF calculations, which

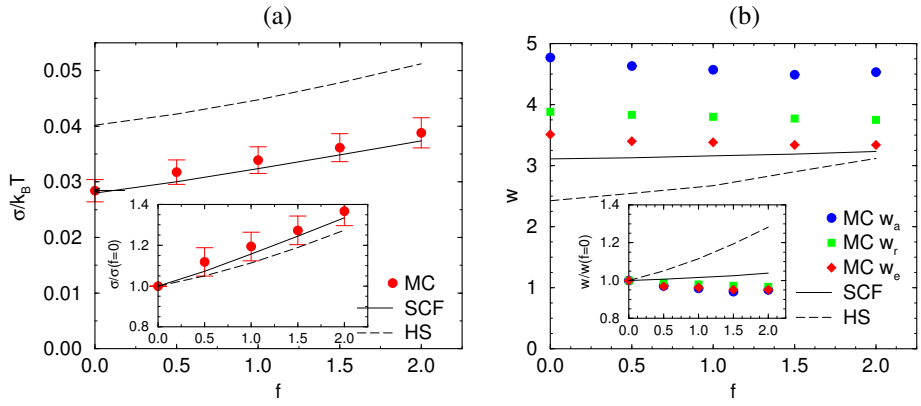

Figure 13. Interfacial tension (**a**) and interfacial width (**b**) in a blend of flexible ($f = 0$) and stiff (f as indicated) polymers at rather strong segregation $\epsilon = 0.05$. Comparisons with detailed SCF calculations, which take account of the chain architecture on all length scales, and predictions of the Gaussian chain model by Helfand and Sapse (HS) are shown. In panel (**b**) w_a denotes the apparent width, which is averaged over the whole lateral system size $L = 64$, w_r represents the width on the block size $B = 16$, and $w_e = 2\Delta e/\chi T\rho$ denotes the width extracted from the excess energy Δe of the interface per unit area, respectively. From Müller and Werner.[25]

enumerate explicit single chain conformations extracted from the MC simulations, predict no increase or even a reduction of the width for larger stiffness, while the intrinsic width increases in the Gaussian chain model. The break down of the Gaussian chain model can be qualitatively rationalized as follows: The width of the interface is determined by loops of the polymers into the other phase. For large incompatibility the width of the interface becomes comparable with the persistence length and the conformation of a loop differs from the Gaussian statistic of the chain on large length scales. Likewise, MC simulations, SCF calculations and predictions of the Gaussian chain model agree for smaller χ, where $w \gg b$.

The ability of the SCF calculations to provide a detailed description of the intrinsic interface structure is illustrated in Fig.14. We present the MC and SCF results for the orientations as measured by the 2^{nd} Legendre polynom of the angle between the bond vector or end–to–end distance $\boldsymbol{R_e}$ with respect to the interface. Both vectors align parallel to the interface, but the effect is much stronger for $\boldsymbol{R_e}$ and more stiffness dependent for the bond vectors.

Diblock copolymers are model surfactants for the AB homopolymer blend. They adsorb at the interface as to extend both halves into the corresponding homopolymer phases. This decreases their enthalpy, but the localization at the interface reduces the translational entropy and the conformational entropy due to chain stretching at high copolymer excess at the interface. Upon increasing the chemical potential $\delta\mu$ (or concentration) of the copolymers in the bulk, we observe the adsorption of copolymers at the interface and the concomitant reduction of the interfacial tension in Fig.15 (cf. also Fig.1). Both MC simulations and SCF calculations agree at high segregation. However, rather than forming a dense copolymer brush at the interface, a phase separation into a homopolymer–rich phase and a lamellar phase (swollen by homopolymers) is encountered.

For small ϵ the addition of copolymers drives the system to compatibility (c.f.

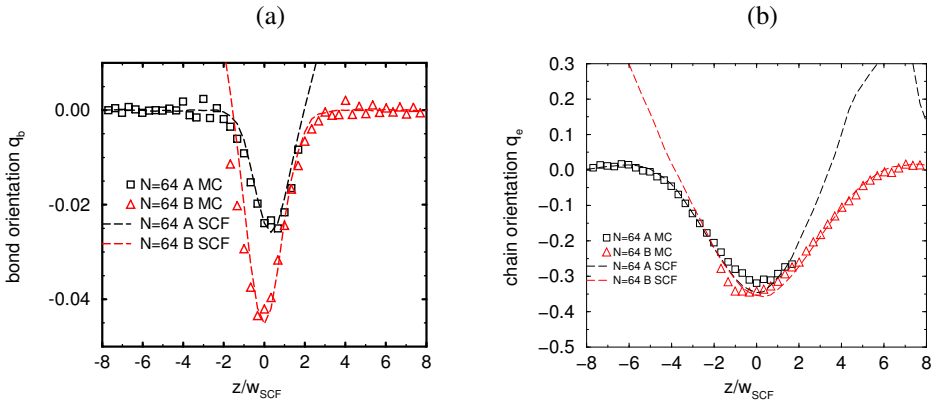

Figure 14. Orientations of the bond vector (**a**) and $\boldsymbol{R_e}$(**b**) in a blend of polymers with stiffness $f = 0$ (left side) and $f = 1$ (right side) at rather strong segregation $\epsilon = 0.05$ and chain length $N = 64$. Symbols denote the results of the MC simulation on a lateral length scale $B = 16$, while lines represent the SCF calculations. From Müller and Werner.[25]

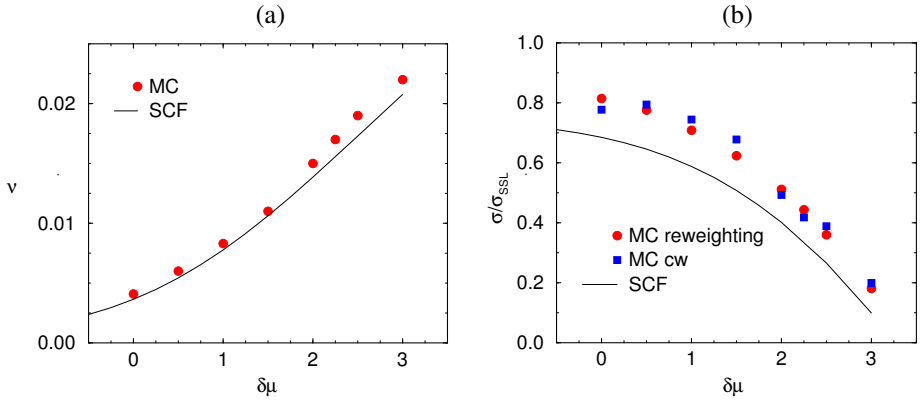

Figure 15. (**a**) Adsorption of diblock copolymers at a homopolymer/homopolymer interface as a function of the chemical potential of the copolymer at $\epsilon = 0.1$ and chain length $N = 32$. (**b**) Reduction of the interfacial tension upon adding copolymers. From Werner et al.[99]

Fig.16(**a**)). At intermediate segregation we find a three phase coexistence between two homopolymer–rich phases and a copolymer–rich disordered phase. The latter has a structure of a microemulsion (as revealed, e.g., by snapshots). SCF calculations by Janert and Schick[100] rather predict highly swollen lamellar phases in this region. Some insight into this discrepancy can be gained from the spectrum of interface fluctuations. Upon adding copolymers to the systems at $\epsilon = 0.054$ we decrease the interfacial tension and deviations from a simple q^2 dependence become apparent (see panel (**b**)). We can obtain a rough estimate of the bending rigidity κ of the copolymer-loaden interface according to Eq.(37). The bending rigidity turns out to be much smaller than $T/2\pi$. It is this bending rigidity, however, which stabilizes the liquid–crystalline order of the lamellar phase. De Gennes and Taupin[101] argued that a small value of κ leads to the formation of a microemulsion. Indeed this is observed in the simulation[102] and experiments.[103] If we were to increase the

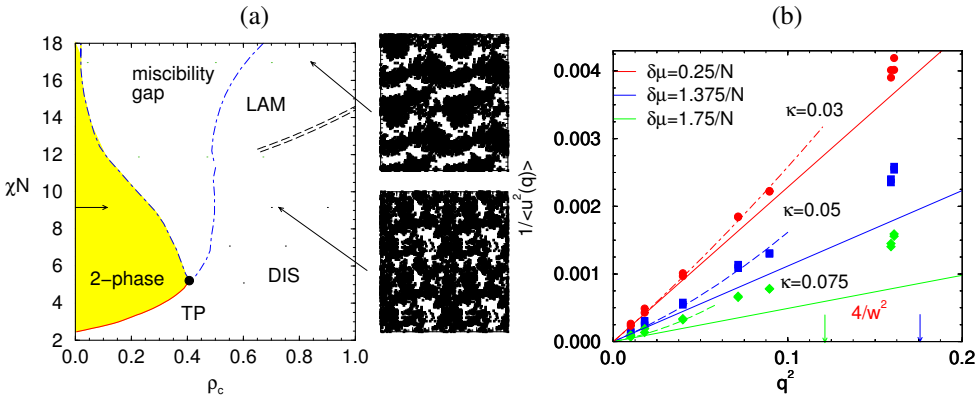

Figure 16. (**a**) Isopleth cut through the phase triangle of a ternary blend. (**b**) Spectrum of interface fluctuations in a ternary blend of two homopolymers and a diblock copolymer at $\epsilon = 0.054$. Estimates for the bending rigidity of the interfaces are indicated. From Müller and Schick.[42]

chain length we would increase the bending rigidity $\kappa \sim \sqrt{N}$[104] and stabilize the lamellar phases predicted by the SCF theory. This reasoning agrees with the Ginzburg criterium at the (tricritical) Lifshitz point.[105]

Acknowledgments

It is a great pleasure to thank Anna Cavallo for a critical reading of the manuscript. Fruitful and enjoyable collaborations with K. Binder, A. Cavallo, M. Fuchs, L. Schäfer, M. Schick, F. Schmid, A. Werner, financial support from the DFG under grants Mu1674/1 and access to the CRAY T3Es at the NIC Jülich and the HLR Stuttgart are acknowledged.

References

1. C. Solc, (edt.) *Polymer Compatibility and Incompatibility, Principles and Practices*, Haarwood Academic, Chur, (1980). C.D. Han (edt.) *Polymer Blends and Composites in Multiphase Systems*, ACS, Washington D.C. R.W. Cahn, P. Haasen, and E.J. Kramer, *Materials Science and Technology, A Comprehensive Treatment*, Vol 12, VCH, Weinheim (1993). D.R. Paul and S. Newman, *Polymer blends*, AP, New York (1978). D.S. Walsh, J.S. Higgins and A. Maconnachie, *Polymer blends and mixtures*, Martinus Nijhoff Publishers, Dordrecht (1985).
2. C. Creton, E.J. Kramer, and G. Hadziioannou, Macromolecules **24**, 1846 (1991).
3. G.I. Taylor, Proc.R.Soc. London, **A 138**, 41 (1932).
4. S.T. Milner, MRS Bull. **22**, 38 (1997).
5. P. Van Konynenburg and R.L. Scott, Philos Trans Soc London Series **A298**, 495 (1980).
6. E. Helfand, Y. Tagami, J.Chem.Phys. **56**, 3592 (1972); E. Helfand, J.Chem.Phys. **62**, 999 (1975).
7. J. Noolandi, K.M. Hong, Macromolecules **14**, 727 (1981); *ibid* **15**, 483 (1982).

8. K.R. Shull, Macromolecules **26**, 2346 (1993).
9. J.M.H.M. Scheutjens, G.J. Fleer, J.Phys.Chem. **83** ,1619 (1979); *ibid* **84** , 178 (1979); Macromolecules **18**, 1882 (1985).
10. M.W. Matsen and M. Schick, Phys.Rev.Lett. **74**, 4225 (1995).
11. M.L. Huggins, J.Chem.Phys. **9**, 440 (1941); P.J. Flory, J.Chem.Phys. **9**, 660 (1941).
12. K.S. Schweizer and J.G. Curro, Advances in Chemical Physics, **XCVIII**, 1 1997. Prigogine and S.A.Rice (eds.), Wiley.
13. K.W. Foreman and K.F. Freed, Advances in Chemical Physics **103**, 335 (1998); K.F. Freed and J. Dudowicz, Macromolecules **31**, 6681 (1998).
14. A. Sariban and K. Binder, Macromolecules **21**, 711 (1988); **24**, 587 (1991); J.Chem.Phys. **86**, 5859 (1987); Makromol.Chem. **189**, 2357 (1988).
15. F.S. Bates, M.F. Schultz, J.H. Rosedale, and K. Almdal, Macromolecules **25**, 5547 (1992); M.D. Gehlsen and F.S. Bates, Macromolecules **27**, 3611 (1994); F.S. Bates and G.H. Fredrickson, Macromolecules **27**, 1065 (1994).
16. D. Schwahn, G. Meier, K. Mortensen, and S. Janssen, J.de.Phys. II (France) **4**, 837 (1994); H. Frielinghaus, D. Schwahn, L. Willner, and T. Springer, Physica **B 241**, 1022 (1998).
17. P. Cifra, E. Nies, and J. Broersma, Macromolecules **29**, 6634 (1996); P. Cifra, F.E. Karasz, and W.J. MacKnight, Macromolecules **25**, 192 and 4895 (1992).
18. H.-P. Deutsch and K. Binder, Europhys. Lett. **18**, 667 (1992); Macromolecules **25**, 6214 (1992); J.Phys. II (France) **3** 1049 (1993).
19. M. Müller and K. Binder, J.Phys. II (France) **6**, 187 (1996).
20. M. Murat and K. Kremer, J.Chem.Phys. **108**, 4340 (1998).
21. D. Heine, D.T. Wu, J.G. Curro, and G.S. Grest, J.Chem.Phys. **118**, 914 (2003).
22. M. Müller, Macromolecules **31**, 9044 (1998).
23. K.A. Peterson, A.D. Stein, and D.M. Fayer, Macromolecules **23**, 111 (1990).
24. I. Szleifer, A. Ben-Shaul, and W.M. Gelbhart, J.Chem.Phys. **1986**, **85**, 5345 (1986). *ibid.* **86**, 7094 (1987). I. Szleifer and M.A. Carignano, Adv. Chem. Phys. **94**, 742 (1996).
25. M. Müller and A. Werner, J.Chem.Phys. **107**, 10764 (1997).
26. P.G. de Gennes, *Scaling concepts in polymer physics*, Cornell University Press, **1979**, Ithaca.
27. I.M. Lifshitz, A.Y. Grosberg, and A.R. Khokhlov, Rev.Mod.Phys **50**, 683 (1978).
28. J.K. Maranas, M. Momdello, G.S. Grest, S.K. Kumar, P.G. Debenedetti, W.W. Graessley, Macromolecules **31**, 6991 and 6998 (1998); J.D. Londono, J.K. Maranas, M. Mondello, A. Habenschuss, G.S. Grest, P.G. Debenedetti, W.W. Graessley, S.K. Kumar, J.Poly.Sci. **B 36**, 3001 (1998).
29. I. Carmesin and K. Kremer, Macromolecules **21**, 2819 (1988); H.-P. Deutsch and K. Binder, J.Chem.Phys. **94**, 2294 (1991).
30. V. Tries, W. Paul, J. Baschnagel, and K. Binder, J.Chem.Phys. **106**, 738 (1997).
31. N.F. Carnahan and K.E. Starling, J.Chem.Phys. **51**, 635 (1969). H.-P. Deutsch and R. Dickman, J.Chem.Phys. **93**, 8983 (1990).
32. M. Müller and K. Binder, Macromolecules **28**, 1825 (1995); M. Müller and K. Binder, Computer Phys. Comm. **84**, 173 (1994).
33. K. Kremer and K. Binder, Comp.Phys.Rep. **7**, 261 (1988).
34. W.G. Madden, A.I. Pesci, and K.F. Freed, Macromolecules **23**, 1181 (1990).

35. P. Cifra, K.F. Karasz, and W.J. McKnight, Macromolecules **25**, 4895 (1992); E. Nies and P. Cifra, Macromolecules **27**, 6033 (1994).
36. S.K. Kumar, Macromolecules **27**, 260 (1994); S.T. Cui, H.D. Cochran, P.T. Cummings, and S.K. Kumar, Macromolecules **27**, 3375 (1997).
37. S.K. Kumar, I. Szleifer, and A.Z. Panagiotopoulos, Phys.Rev.Lett. **66**, 2935 (1991) and Phys.Rev.Lett. **68**, 3456 (1992).
38. F.A. Escobedo and J.J. dePablo, Europhys. Lett. **40**, 111 (1997); F.A. Escobedo and J.J. dePablo, J.Chem.Phys. **106**, 2911 (1997).
39. D.A. Kofke, J.Chem.Phys. **98**, 4149 (1993).
40. R.D. Kaminski, J.Chem.Phys. **101**, 4986 (1994).
41. M. Müller, K. Binder, and W. Oed, J.Chem.Soc.Faraday Trans. **91**, 2369 (1995).
42. M. Müller and M. Schick, J.Chem.Phys. **105**, 8885 (1996).
43. M. Müller and N.B. Wilding, Phys.Rev. **E 51**, 2079 (1995).
44. A.M. Ferrenberg and R. Swendsen, Phys.Rev.Lett. **61**, 2635 (1988).
45. A.M. Ferrenberg and R. Swendsen, Phys.Rev.Lett. **63**, 1195 (1989).
46. B. Berg, J.Stat.Phys. **82**, 323 (1996).
47. F. Wang and D.P. Landau, Phys.Rev.Lett. **86**, 2050 (2001).
48. Q. Yan and J.J. de Pablo, Phys.Rev.Lett. **90**, 035701 (2003).
49. U. Hansmann and L. Wille, Phys.Rev.Lett. **88**, 068105 (2002).
50. B. Schulz, K. Binder, and M. Müller, J.Mod.Phys. **C 13**, 477 (2002).
51. J.S. Wang, T. Tay, and R. Swendsen, Phys.Rev.Lett. **82**, 476 (1999).
52. G. Smith and A. Bruce, J.Phys. **A 28**, 6623 (1995).
53. P. Virnau and M. Müller (preprint, 2003).
54. M.D. Gehlen, J.H. Rosedale, F.S. Bates, G.D. Wignall, K. Almdal, Phys.Rev.Lett. **68**, 2452 (1992).
55. A. Yethiraj and K.S. Schweizer, J.Chem.Phys. **97**, 5927 (1992) and **98**, 9080 (1993); K.S. Schweizer and A. Yethiraj, J.Chem.Phys. **98**, 9053 (1993); C. Singh, K.S. Schweizer, and A. Yethiraj, J.Chem.Phys. **102**, 2187 (1995).
56. M. Müller, Macromol.Theory Simul. **8**, 343 (1999).
57. V.L. Ginzburg, Sov.Phys.Solid State **1**, 1824 (1960); P.G. de Gennes, J.Phys.Lett. (Paris) **38**, L-441 (1977); J.F. Joanny, J.Phys.A **11**, L-117 (1978); K. Binder, Phys.Rev.A **29**, 341 (1984).
58. M.E. Fisher, Rev.Mod.Phys. **46**, 587 (1974); K.K. Mon and K. Binder, Phys.Rev. **E 48**, 2498 (1993).
59. G.S. Grest, M.-D. Lacasse, K. Kremer, A.M. Gupta, J.Chem.Phys. **105**, 10583 (1996).
60. F.A. Escobedo and J.J. dePablo, Macromolecules **32**, 900 (1999).
61. A. Cavallo, M. Müller, and K. Binder, Europhys. Lett. **61**, 214 (2003).
62. A.J. Silverberg, Colloid Interface Sci **90**, 86 (1982).
63. Since we focus on semi–dilute solutions (and melts), we express all quantities for $r > \xi_{\rm ev}$ in terms of R_e and $\mathcal{N}$. Conceiving a chain as a random walk of blobs of size $\xi_{\rm ev}$, we can write: $R^2 = b^2 N \sim \xi_{\rm ev}^2 N/g$ where g is the number of monomeric units per blob. To a first approximation, blobs do not interdigitate and $g \sim \rho\xi_{\rm ev}^3$. Then we obtain $\xi \sim 1/\rho b^2 = R_e/(\sqrt{\mathcal{N}})$. To make contact with the dilute limit, we use $R_0 \sim b_{\rm ev} N^{\nu_{\rm ev}}$ with $\nu_{\rm ev} = 0.588$ for the chain extension in the limit $\rho \to 0$, and we define the overlap $s = \rho R_0^3/N$. The extension in semi-dilute solutions is related to the properties in the dilute limit via: $R_e^2 \sim R_0^2 \mathcal{F}(s) \stackrel{s\to\infty}{\to}$

$R_0^2 s^{(1-2\nu_{\rm ev})/(3\nu_{\rm ev}-1)} \sim b_0(\rho b_0^3)^{(1-2\nu_{\rm ev})/(3\nu_{\rm ev}-1)} N$. Using this limiting scaling behavior we find for the screening length $\xi_{\rm ev} \sim R_e/\sqrt{\mathcal{N}} \sim b_0(\rho b_0^3)^{\nu_{\rm ev}/(1-3\nu_{\rm ev})}$ and for the overlap $s \sim \mathcal{N}^{3\nu_{\rm ev}-1}$.

64. M. Müller and K. Binder, Macromolecules **31**, 8323 (1998).
65. M. Müller, K. Binder, E.V. Albano, Int.J.Mod.Phys. **B15**, 1867 (2001).
66. K. Binder, D.P. Landau, M. Müller, J.Stat.Phys. **110**, 1411 (2003).
67. M. Müller, Macromolecules **28**, 6556 (1995).
68. M. Dijkstra and D. Frenkel, Phys.Rev.Lett. **72**, 292 (1994); M. Dijkstra, D. Frenkel, and J.P. Hansen, J.Chem.Phys. **101**, 3179 (1996).
69. W.W. Graessley, R. Krishnamoorti, N.P. Balsara, L.J. Fetters, D.J. Lohse, D.N. Schulz, and J.A. Sissano, Macromolecules **27**, 2574, 3073 and 3896 (1994); R. Krishnamoorti, W.W. Graessley, G.T. Dee, D.J. Walsh, L.J. Fetters, and D.J. Lohse, Macromolecules **29**, 367 (1996); G.C. Reichart, W.W. Graessley, R.A. Register, R. Krishnamoorti, and J.D. Lohse, Macromolecules **30**, 3036 (1996); W.W. Graessley, R. Krishnamoorti, G.C. Reichart, N.P.Balsara, L.J. Fetters, and D.J. Lohse, Macromolecules **28**, 1260 (1995); R. Krishnamoorti, W.W. Graessley, L.J. Fetters, R.G. Garner, and D.J. Lohse, Macromolecules **28**, 1252 (1995).
70. J.H. Hildebrand and R.L. Scott, *The solubility of nonelectrolytes*, Dover Publications, New York (1964); J.H. Hildebrand, J.M. Prausnitz, R.L. Scott, *Regular and related solutions*, Van Nostrand Reinhold Co., New York (1970).
71. J.P. Wittmer, W. Paul, and K. Binder, Macromolecules **25**, 7211 (1992).
72. G.H. Fredrickson, A.J. Liu, and F.S. Bates, Macromolecules **27**, 2503 (1994). G.H. Fredrickson and A.J. Liu, J.Polym.Sci. **B33**, 1203 (1995).
73. C. Singh and K.S. Schweizer, Macromolecules **28**, 8692 (1995); J.Chem.Phys. **103**, 5814 (1995); Macromolecules **30**, 1490 (1997); K.S. Schweizer and C. Singh, Macromolecules **28**, 2063 (1995).
74. K.W. Foreman and K.F. Freed, Macromolecules **30**, 7279 (1997); K.W. Foreman, K.F. Freed, and I.M. Ngola, J.Chem.Phys. **107**, 4688 (1997); K.F. Freed and J. Dudowicz, Macromolecules **29**, 625 (1996).
75. J.D. Weinhold, S.K. Kumar, C. Singh, and K.S. Schweizer, J.Chem.Phys. **103**, 9460 (1995).
76. S.K. Kumar and J. Weinhold, Phys.Rev.Lett. **77**, 1512 (1996).
77. J. Dudowicz, K.F. Freed, and J.F. Douglas, J.Chem.Phys. **116**, 9983 (2002); Phys.Rev.Lett. **88**, 095503 (2002).
78. M. Rabeony, D.J. Lohse, R.T. Garner, S.J. Han, W.W. Graessley, and K.B. Migler, Macromolecules **31**, 6511 (1998).
79. M. Müller and W. Paul, J.Chem.Phys, **100**, 719 (1994).
80. J.K. Taylor-Maranas, P.G. Debenedetti, W.W. Graessley, and S.K. Kumar, Macromolecules **30**, 6943 (1997).
81. J.F. Joanny and H. Benoit, Macromolecules **30**, 3704 (1997); J.F. Joanny, H. Benoit, and W.H. Stockmayer, Macromol.Symp. **121**, 95 (1997).
82. D.G. Gromov and J.J. dePablo, J.Chem.Phys. **109**, 10042 (1998).
83. M. Müller, K. Binder, and L. Schäfer, Macromolecules **33**, 4568 (2000).
84. M. Fuchs and M. Müller, Phys. Rev. **E 60**, 1921 (1999).
85. J.-F. Joanny, L. Leibler, and R Ball, J.Chem.Phys. **81**, 4640 (1984)..
86. L. Schäfer and C. Kappeler, J.Chem.Phys. **99** 6135 (1993); L. Schäfer and C. Kap-

peler, J.Phys. (France) **46**, 1853 (1985).
87. C.J. Grayce, A. Yethiraj, K.S. Schweizer, J.Chem.Phys. **100**, 6857 (1994). C.J. Grayce, K.S. Schweizer, J.Chem.Phys. **100**, 6846 (1994).
88. J.D. Weinhold, J.G. Curro, A. Habenschuss, J.D. Londono, Macromolecules **32**, 7276 (1999).
89. F. Eurich and P. Maass, J.Chem.Phys. **114**, 7655 (2001).
90. R. Holyst and T.A. Vilgis, Macromol.TheorySimul, **5**, 573 (1996).; R. Holyst and T.A. Vilgis, J.Chem.Phys. **99**, 4835 (1993); Phys.Rev.E **50**, 2087 (1994); M.G. Brereton and T.A. Vilgis, J.Phys. (France) **50**, 245 (1989); A. Aksimentiev and R. Holyst, Macromol. Theory Simul. **7**, 447 (1998).
91. G.E. Garas and M.K. Kosmas, J.Chem.Phys. **103**, 10790 (1995); *ibid* **105**, 4789 (1996); *ibid* **108**, 376 (1998); M.K. Kosmas, Macromolecules **22**, 720 (1989).
92. A.N. Semenov, J.Phys. II **6**, 1759 (1996).
93. F. Schmid and M. Müller, Macromolecules **28**, 8639 (1996).
94. A. Werner, F. Schmid, M. Müller, and K. Binder, Phys.Rev. **E 59**, 728 (1999).
95. A. Werner, F. Schmid, M. Müller, and K. Binder, J.Chem.Phys. **107**, 8175 (1997).
96. M.D. Lacasse, G.S. Grest, and A.J. Levine, Phys.Rev.Lett. **80**, 309 (1998).
97. A.N. Semenov, Macromolecules **27**, 2732 (1994).
98. E. Helfand and A.M. Sapse, J.Chem.Phys. **62**, 1329 (1975).
99. A. Werner, F. Schmid, and M. Müller, J.Chem.Phys. **110**, 5370 (1999).
100. P.K. Janert and M. Schick, Macromolecules **30**, 3916 (1997).
101. P.G. de Gennes and C. Taupin J.Phys.Chem. **86**, 2294 (1982).
102. M. Müller and M. Schick, J.Chem.Phys. **105**, 885 (1996).
103. G.H. Fredrickson and F.S. Bates, Polym.Sci. **B 35**, 2775 (1997).
H.S. Jeon, J.H. Lee, and N.P. Balsara, Phys.Rev.Lett. **79**, 3274 (1997).
104. M.W. Matsen, J.Chem.Phys. **110**, 4658 (1999).
105. M. Müller and G. Gompper, Phys.Rev. **E 66**, 041805 (2002).